Thymic macrophages consist of two populations with distinct localization and origin

Tyng-An Zhou[1], Hsuan-Po Hsu[1], Yueh-Hua Tu[2,3], Chih-Yu Lin[1], Nien-Jung Chen[1], Jin-Wu Tsai[4], Ellen A. Robey[5], Hsuan-Cheng Huang[2,6], Chia-Lin Hsu[1], and Ivan L. Dzhagalov[1*]

[1]Institute of Microbiology and Immunology, National Yang-Ming University, Taipei, Taiwan

[2]Bioinformatics Program, Taiwan International Graduate Program, Institute of Information Science, Academia Sinica, Taipei, Taiwan

[3]Graduate Institute of Biomedical Electronics and Bioinformatics, National Taiwan University, Taipei, Taiwan

[4]Brain Research Center, National Yang-Ming University, Taipei, Taiwan

[5]Division of Immunology and Pathogenesis, Department of Molecular and Cell Biology, University of California, Berkeley, CA, United States

[6]Institute of Biomedical Informatics, National Yang-Ming University, Taipei, Taiwan

*Correspondence to Ivan L. Dzhagalov: ivan.dzhagalov@nycu.edu.tw, ORCID: 0000-0001-9209-4582

Mailing Address: Ivan L. Dzhagalov, Institute of Microbiology and Immunology, National Yang-Ming Chiao-Tung University, #155, Sec. 2, LiNong Street, Beitou, Taipei City, 11221, TAIWAN

Abstract

Tissue-resident macrophages are essential for protection from pathogen invasion and maintenance of organ homeostasis. The ability of thymic macrophages to engulf apoptotic thymocytes is well appreciated, but little is known about their ontogeny, maintenance, and diversity. Here, we characterized the surface phenotype and transcriptional profile of these cells and found out that they express typical tissue-resident macrophage genes yet also exhibit organ-specific features. Thymic macrophages were most closely related to spleen red pulp macrophages and Kupffer cells and shared the expression of the transcription factor SpiC with these cells. Using shield chimeras, transplantation of embryonic thymuses, and fate mapping, we found that three distinct waves of precursors generate thymic macrophages. Moreover, some of them proliferated in situ. Single-cell RNA sequencing showed that the macrophages in the adult thymus are composed of two populations with distinct localization and origin. Altogether, our work defines the phenotype, origin, and diversity of thymic macrophages.

Introduction

Tissue-resident macrophages are present in every organ and maintain local homeostasis through diverse functions ranging from protection against pathogens to tissue repair[1]. To perform their roles efficiently, macrophages acquire specialized phenotypes depending on the tissue microenvironment, and as a consequence, multiple subtypes exist, frequently within the same organ. For example, the spleen harbors red pulp macrophages specialized in red blood cell phagocytosis, marginal zone macrophages and metallophilic macrophages that are the first defense against blood-borne pathogens, T cell zone macrophages that silently dispose of apoptotic immune cells, and tingible-body macrophages that engulf less fit B cells in the germinal center[2-4]. Thus, tissue-resident macrophages represent a fascinating developmental system that allows enormous plasticity.

The last decade has seen a paradigm shift in our understanding of the development of tissue-resident macrophages. Contrary to the long-held belief that all macrophages derive from circulating monocytes[5], multiple studies have shown that many of them are long-lived cells with an embryonic origin that can maintain themselves in the tissues (reviewed in[6]). Three waves of distinct progenitors settle the tissues and contribute in various degrees to the resident macrophages in each organ. The first wave consists of yolk sac (YS)-derived primitive macrophages that enter all tissues and establish the earliest macrophage populations[7,8]. In all organs, except for the brain and, partially, the epidermis, primitive macrophages are replaced by the next wave consisting of fetal monocytes[9-12]. The third wave comes from hematopoietic stem cell (HSC)-derived monocytes that contribute to various degrees to the

macrophage pool in different tissues. For example, these cells contribute little to the microglia in the brain, Langerhans cells in the epidermis, and alveolar macrophages in the lungs but substantially to most other organs[13-16]. Moreover, the kinetics and timing of HSC-derived monocytes infiltration vary in different parts of the body. For some macrophage populations, such as the arterial macrophages and subcapsular lymph node macrophages, monocytes replace embryonic macrophages soon after birth and self-maintain after that with little contribution from circulating cells[17,18]. Others, such as heart macrophages, osteoclasts, and pancreatic isles macrophages are progressively replaced at a low rate[14,19-23]. A third group, such as the macrophages in the dermis and most of the gut macrophages, are constantly replaced by blood monocytes with relatively fast kinetics[24,25]. These conclusions have been extended to many different macrophage populations such as Kupffer cells, liver capsular macrophages, red pulp macrophages, testicular macrophages, large and small peritoneal macrophages, and T zone macrophages in the lymph nodes[2,13,14,16,26-30].

The recent revitalization in macrophage research has yet to reach thymic macrophages. Although their prodigious phagocytic ability is well appreciated[31], little is known about the origin, diversity, and maintenance of these cells. This gap in our knowledge is, in part, due to the lack of a consensus about the surface phenotype of thymic macrophages. Various groups have used different markers to identify these cells, such as F4/80 and Mac-3 (LAMP-2)[31], or CD4 and CD11b[32], or Mac-2 (galectin 3), F4/80 and ED-1 (CD68)[33]. Most commonly, researchers employ F4/80 and CD11b[34-37]. However, none of these markers is macrophage-specific: F4/80 is also

91 expressed on eosinophils and monocytes[38,39], while CD11b is present on
92 most myeloid cells. The lack of a clear phenotypic definition of thymic
93 macrophages has translated into the absence of models that target genes
94 specifically in this population. For example, although macrophages in various
95 organs have been successfully targeted with *Lyz2*^{Cre}, *Csf1r*^{Cre}, or *Cx3cr1*^{Cre},
96 very few studies have used these models in the thymus[37,40,41].
97 Only a handful of studies has explored the origin of thymic macrophages.
98 Several reports have indicated that these cells could be derived from T cell
99 progenitors in the thymus based on an improved single cell in vitro culture and
100 in vivo transplantation experiments[42,43]. However, these conclusions have
101 been questioned based on fate-mapping experiments using *Il7r*^{Cre} that found
102 very limited contribution of lymphoid progenitors to thymic macrophages in
103 vivo in unperturbed mice[44]. Most recently, Tacke et al. used parabiosis to
104 rule out circulating monocytes as a major source for thymic macrophages[37].
105 The same study also performed fate-mapping experiments to show that most
106 thymic macrophages descend from *Flt3*$^{+}$ HSC-derived progenitors. However,
107 the contribution of earlier waves of hematopoiesis has not been explored.
108 Here, we aimed to bring our knowledge of thymic macrophages on par with
109 other tissue-resident macrophages. We started by providing a clear definition
110 of thymic macrophages according to the guidelines set by the Immunological
111 Genome Consortium (IMMGEN)[38] and characterized their surface
112 phenotype and transcriptional signature. Using single-cell RNA sequencing
113 (scRNA-Seq), we identified two populations of thymic macrophages with
114 distinct localization. We explored the origin of these cells through genetic fate
115 mapping, shield chimeras, and embryonic thymus transplantation and

116 documented that three separate waves of progenitors give rise to resident
117 thymic macrophages. Altogether our work fills an important gap in our
118 understanding of resident thymic macrophages and provides the framework
119 for future functional characterization of these cells.
120
121 **Results:**
122 **CD64, F4/80, and MerTK identify the macrophages in the thymus**
123 To unambiguously and comprehensively identify macrophages in the
124 thymus, we evaluated several of the prototypical macrophage markers,
125 MerTK, CD64, and F4/80[38]. Only MerTK identified a population that stained
126 completely with the other two markers (Fig. 1a). F4/80 labeled Siglec $F^{+}SSC^{hi}$
127 eosinophils and $CD64^{+}CD11b^{+}$ monocytes, in addition to $MerTK^{+}$ cells (Fig.
128 S1a). CD64 identified $CD11b^{+}F4/80^{lo}$ monocytes (Fig. S1b). Thus, MerTK
129 appeared to be the best marker for macrophages in the thymus. However,
130 staining with MerTK and F4/80 was relatively dim even when the brightest
131 fluorochromes (e.g., PE) were used and could not be resolved fully from the
132 isotype control (Fig. S1c). For practical purposes, to identify macrophages,
133 we used CD64 together with F4/80 and CD11b to exclude monocytes (Fig.
134 S1d). In addition, we also employed forward scatter (cells size) to exclude
135 cells that appeared $MerTK^{+}$, $CD64^{+}$, $F4/80^{+}$, but were much smaller and less
136 granular than the rest of the macrophages, and many of them were $Thy1^{+}$
137 (Fig. S1e).
138 The $CD64^{+}F4/80^{+}MerTK^{+}CD11b^{lo}FSC^{hi}$ cells had typical macrophage
139 morphology with abundant cytoplasm (Fig. 1b). These cells did not express
140 lineage markers characteristic of T cells (CD3ε), B cells (CD19), eosinophils

141 (Siglec F), NK cells (NK1.1), neutrophils (Gr1), or plasmacytoid dendritic cells
142 (Siglec H) (Fig. 1c). However, they expressed phagocytic receptors such as
143 TIM4, CD51, and Axl (Fig. 1d).

144 To ascertain that our gating strategy identifies all macrophages in the
145 thymus in an unbiased way, we performed scRNA-Seq of sorted *Csf1r*$^{GFP+}$
146 and *Cd11c*$^{YFP+}$ thymic cells. *Csf1r* is required for the survival of most
147 macrophages and is considered their definitive marker[45,46], while *Cd11c*^{YFP}
148 is expressed in many myeloid cells, including macrophages[47]. Both
149 reporters identified an overlapping set of cells (Fig. S2a). Two clusters
150 expressed the macrophage/monocytes-specific transcription factor *Mafb* and
151 high levels of *Fcrg1* (CD64), *Mertk*, and *Adgre1* (F4/80), indicating that they
152 are macrophages (Fig. 1e). An additional cluster expressed *Mafb* together
153 with *Fcgr1* and *Adgre1* but not *Mertk*, fitting the description of monocytes.
154 Altogether the scRNA-Seq data confirmed that our flow cytometry gating had
155 identified all macrophages in the thymus. Importantly, MerTK^{+} cells could not
156 be labeled by intravenously injected CD45 antibody (Fig. 1f), proving that they
157 reside in the parenchyma of the organs and not in the blood vessels. Based
158 on the above data, we will refer to CD64^{+}F4/80^{+}MerTK^{+}CD11b^{lo}FSC^{hi} cells as
159 thymic macrophages. The smaller CD64^{+}F4/80^{lo}CD11b^{+}FSC^{hi} population did
160 not express MerTK, but most of them expressed Ly6C, and we classify them
161 as thymic monocytes.

162 Thymic macrophages expressed CD11c, MHC2, and SIRPα that made
163 them partially overlap with CD11c^{+}MHC2^{+} classical dendritic cells (cDCs),
164 thus making problematic the unambiguous identification of thymic cDCs
165 based only on these two markers (Fig. S1f). Proper identification of cDC in the

166 thymus requires the exclusion of macrophages based on CD64 or MerTK
167 staining. Otherwise, the cDCs, particularly the SIRPα^+ cDC2 subset, would
168 be contaminated with macrophages that account for ~25% of cDC2 (Fig.
169 S1g).
170 Thymic macrophages were ~0.1% of all the cells in the thymus of young
171 adult mice and numbered ~4x10^5 on average per mouse (Fig. 1g). We did not
172 find statistically significant differences in their percentages between 4 and 11
173 weeks of age. Still, there was a significant decline in their numbers with age,
174 consistent with the beginning of thymic involution (Fig. 1h).
175 To determine if thymic macrophages are avid phagocytes, we evaluated
176 their participation in the phagocytosis of apoptotic cells in the thymus by
177 TUNEL staining. We used TIM4 and MerTK as single stains to identify
178 macrophages in tissue sections because they are not expressed on any other
179 cell type in the thymus instead of following our multiple-label flow cytometry
180 strategy. Most of the TUNEL$^+$ cells could be found clearly inside or closely
181 associated with MerTK$^+$ and TIM4$^+$ cells in the thymus (Fig. S3a and b). On
182 average, ~85% of all TUNEL$^+$ cells were within 5 μm of MerTK$^+$ cells,
183 indicating that thymic macrophages are the major phagocytic population in the
184 thymus (Fig. S3c). The degree of co-localization between TUNEL$^+$ cells and
185 TIM4$^+$ cells was slightly lower, ~75% on average, possibly reflecting the
186 absence of TIM4 expression on a small proportion of thymic macrophages
187 (Fig. 1d).

188

189

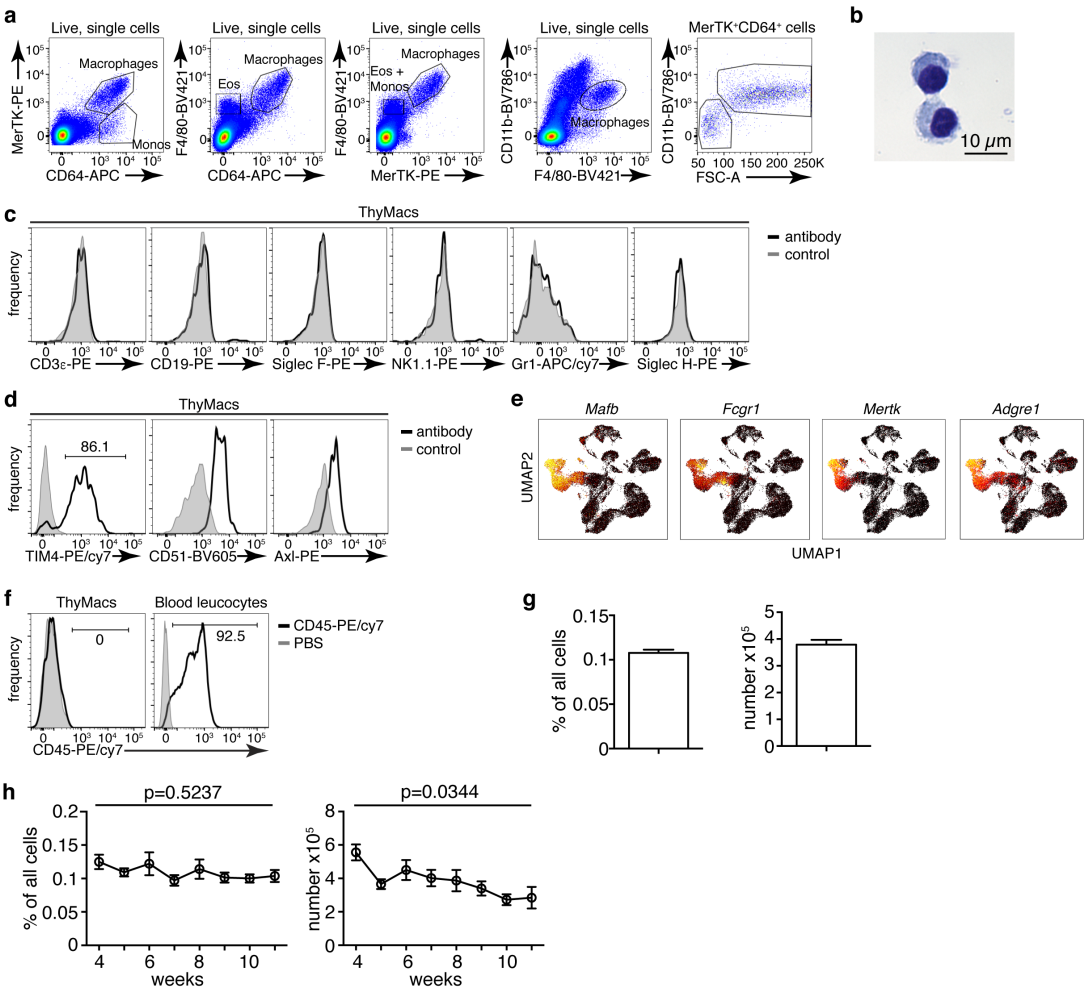

Figure 1. Thymic macrophages (ThyMacs) can be identified by the expression of CD64, MerTK and F4/80. a Flow cytometric analysis of enzymatically digested thymus tissue with macrophage markers CD64, MerTK, F4/80, and CD11b. More details about the confirmation of the identities of eosinophils and monocytes can be found in Fig. S1a and b. **b** Pappenheim (Hemacolor Rapid staining kit) staining of sorted ThyMacs. **c** Lack of expression of lineage markers associated with other cell types on ThyMacs. **d** The expression on ThyMacs of three receptors for phosphatidylserine that participate in the phagocytosis of apoptotic cells. **e** scRNA-Seq data showing the expression of prototypical macrophage genes *Mafb*, *Fcgr1* (CD64), *Mertk*, and *Adgre1* (F4/80) among thymus cells sorted as *Csf1r*$^{GFP+}$ and *Cd11c*$^{YFP+}$. **f** Labeling of ThyMacs with intravenously

202 injected anti-CD45-PE antibody or PBS. The labeling of blood leucocytes is
203 shown for comparison. **g** Average numbers and percentages of ThyMacs in 4-
204 11 weeks old mice, n=82. **h** Comparison of the numbers and percentages of
205 ThyMacs in mice of different ages, n=82. All flow cytometry plots are
206 representative of at least 3 independent repeats. The numbers in the flow
207 cytometry plots are the percent of cells in the respective gates. Data in **g** and
208 **h** represent mean±SEM. Statistical significance in **h** was determined with one-
209 way ANOVA.

210

211 **Transcriptional signature of thymic macrophages**

212 To further understand the identity and functions of the thymic
213 macrophages, we sorted and subjected them to RNA sequencing analysis as
214 part of the IMMGEN's Open Source Mononuclear Phagocyte profiling.
215 Thymic macrophages displayed a transcription profile consistent with tissue-
216 resident macrophages and did not express genes characteristic of other
217 lineages (Fig. 2a). Then, we examined the expression of the core signature
218 macrophage genes[38] and found that they were enriched in thymic
219 macrophages but not in *Sirpa*$^{+}$ or *Xcr1*$^{+}$ thymic cDCs (Fig. 2b). On the
220 contrary, cDC core signature genes were abundantly expressed in both
221 thymic cDC subsets but not in thymic macrophages. These findings establish
222 that although thymic macrophages and cDCs share the thymic
223 microenvironment and expression of CD11c and MHC2, they have distinct
224 transcriptional profiles.

225 We then compared the gene expression profile of thymic macrophages to
226 that of other well-characterized macrophage populations available from

227 IMMGEN. Because of the abundance of samples, we limited our comparison
228 to only nine types of tissue-resident macrophages under steady-state
229 conditions – splenic red pulp macrophages, Kupffer cells, broncho-alveolar
230 lavage macrophages, large peritoneal cavity macrophages, white adipose
231 tissue macrophages, aorta macrophages, central nervous system microglia,
232 and spinal cord microglia. Hierarchical clustering revealed that thymic
233 macrophages were most closely related to splenic red pulp macrophages and
234 Kupffer cells (Fig. 2c).
235 To better identify the unique functions of thymic macrophages, we looked
236 for genes that were differentially expressed in these cells compared to other
237 tissue-resident macrophages. We set three criteria: 1) high expression in
238 thymic macrophages (>500); 2) >5 fold higher expression than the average
239 value in the nine populations of non-thymic macrophages; 3) expression in
240 thymic macrophages is higher than any non-thymic macrophage samples. A
241 total of 44 genes met these criteria, and we consider them to constitute the
242 transcriptional signature of thymic macrophages (Fig. 2d). These included
243 several degradation enzymes and their inhibitors (*Cst7*, *Mmp2*, *Mmp14*,
244 *Dnase1l3*, *Serpina3g*, *Acp5*), non-classical MHC molecules (*H2-M2*, *H2-Q6*,
245 *H2-Q7*), metabolic enzymes (*Chst2*, *Ass1*, *Kynu*, *Cp*, *Dgat2*, *Sorl1*, *Lap3*),
246 molecules involved in innate immunity (*Ifit2*, *Il18bp*, *Mefv*, *Lgals3bp*) and
247 extracellular signaling molecules and their receptors (*Pdgfa*, *Cxcl16*, *Il2rg*,
248 *Gpr157*). We also looked for transcription factors (TFs) highly expressed in
249 thymic macrophages and could potentially regulate critical gene networks in
250 these cells. A total of 25 TFs were highly expressed in thymic macrophages
251 (>250) and were at least 2-fold higher as compared to the non-thymic

252 macrophages (Table S1). Among them were several TFs involved in type I
253 interferon (IFN-I) signaling (*Stat1*, *Stat2*, *Irf7*, and *Irf8*) and lipid metabolism
254 (*Nr1h3*, *Pparg*, *Srebf1*, and *Rxra*) (Fig. 2e). Notably, *Runx3* that is important
255 for the development and function of cytotoxic T lymphocytes[48], innate
256 lymphoid cells[49], and Langerhans cells[50] was highly expressed in thymic
257 macrophages. *SpiC* that has well-documented roles in the development of red
258 pulp macrophages in the spleen, and bone marrow macrophages[51,52] was
259 also highly expressed in thymic macrophages, further strengthening the
260 argument for the similarity between thymus, spleen and liver macrophages.
261 To confirm the expression of *Spic* in thymic macrophages, we analyzed the
262 thymus of $Spic^{GFP}$ mice[52]. We found that all $Spic^{GFP+}$ cells were
263 macrophages (Fig. S4a and b), making them the most specific thymic
264 macrophage reporter strain compared with $Lyz2^{GFP}$, MAFIA ($Csf1r^{GFP}$),
265 $Cd11c^{YFP}$, and $Cx3cr1^{GFP}$ mice (Fig. S4c-e). However, only ~80% of thymic
266 macrophages were $Spic^{GFP+}$ suggesting heterogeneity within the cells (Fig.
267 S4f and g).
268 Several dominant pathways emerged when we grouped the 500 most
269 highly expressed genes in thymic macrophages according to gene ontology
270 (GO) terms (Fig. 2f). It was notable that five of the ten most highly enriched
271 GO pathways concerned antigen presentation of both exogenous and
272 endogenous antigens. These data complement our flow cytometry findings of
273 expression of MHC2 and suggest that thymic macrophages could be potent
274 antigen-presenting cells and might play a role in negative selection or agonist
275 selection of thymocytes. Two other highly enriched GO pathways were
276 involved in lysosomal biogenesis and functions, highlighting the high capacity

277 of these cells to degrade phagocytosed material. Thus, our transcriptional

278 analysis has revealed that thymic macrophages are bona fide macrophages

279 that bear significant similarity to spleen and liver macrophages and are

280 specialized in lysosomal degradation of phagocytosed material and antigen

281 presentation.

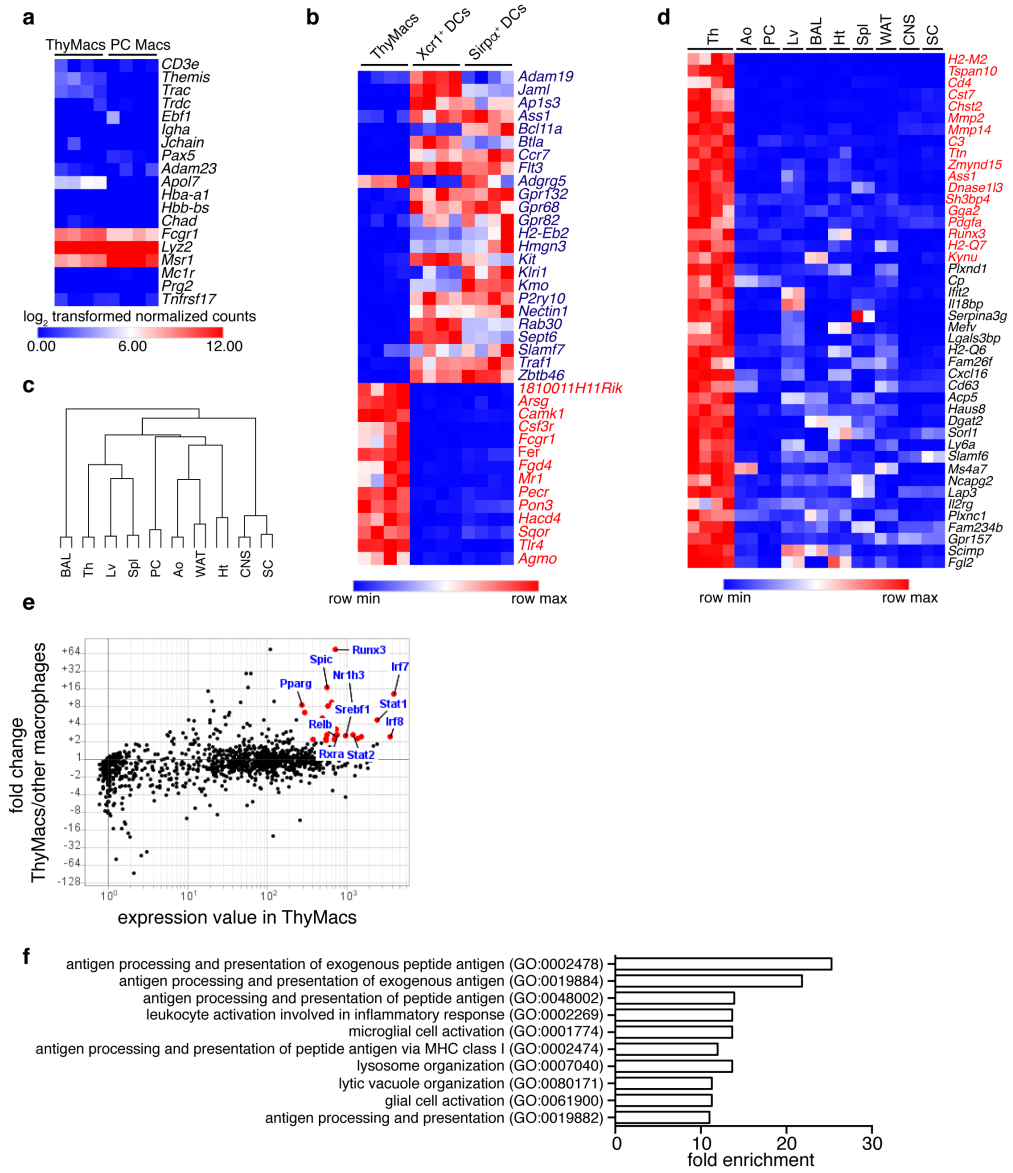

282 **Figure 2. Transcriptional profile of thymic macrophages (ThyMacs). a**

283 Expression of lineage-specific genes in ThyMacs and peritoneal cavity

284 macrophages (PC Macs). **b** Expression of cDC-specific genes (gene names in

285 blue) and macrophage-specific genes (gene names in red) in ThyMacs and

286 two populations of thymic cDCs (ThyDCs) – *Xcr1*$^{+}$ ThyDCs and *Sirpa*$^{+}$

287 ThyDCs. **c** Hierarchical clustering of ThyMacs and nine other populations of
288 tissue-resident macrophages in duplicates. **d** Highly expressed (>500) genes
289 enriched (>5-fold) in ThyMacs (4 samples) compared to nine other tissue-
290 resident macrophage populations (two samples each). The genes in red are
291 >10-fold up-regulated in thymic macrophages. **e** Comparison of the geometric
292 mean expression of transcription factors in thymic macrophages (4 samples)
293 and the nine other macrophage populations (2 samples each). Transcription
294 factors with expression >250 and fold change >2 are marked with red dots. **f**
295 Top 10 GO pathways in ThyMacs based on the 500 most highly expressed
296 genes in these cells. Th – ThyMacs, Spl – spleen red pulp macrophages, Lv –
297 Kupffer cells, BAL – bronchoalveolar lavage macrophages, PC – peritoneal
298 cavity macrophages, Ao – aorta macrophages, Ht – heart macrophages, WAT
299 – white adipose tissue macrophages, CNS – central nervous system
300 microglia, SC – spinal cord microglia.
301

302 **Yolk-sac progenitors contribute to embryonic thymic macrophages**

303 The ontogeny of thymic macrophages has been examined by only one
304 study since the realization that many tissue-resident macrophages are
305 descendants from embryonic progenitors[37]. Based on *Flt3*^{Cre} fate-mapping,
306 the authors concluded that most adult thymic macrophages derive from
307 HSCs. To determine if yolk-sac (YS) progenitors contribute to embryonic
308 thymic macrophages, we used *Cx3cr1*^{CreER} fate mapping[53]. Injection of 4-
309 OHT at E9.5 in *ROSA26*$^{LSL\text{-}GFP}$ mouse mated with a *Cx3cr1*^{CreER} male
310 permanently tags YS progenitors and their descendants with GFP (Fig. 3a).
311 Indeed, E19.5 microglia that are exclusively derived from YS progenitors were

312 labeled to a high degree (Fig. 3b). After adjusting for incomplete labeling
313 based on the microglia, we found that at E15.5 >50% of thymic macrophages
314 were fate mapped, i. e. from YS origin (Fig. 3c). However, GFP^+ thymic
315 macrophages decreased to just ~11% at E19.5, suggesting that YS
316 progenitors establish the embryonic thymic macrophage pool but are quickly
317 replaced by subsequent wave(s) of fetal liver monocytes or HSC-derived
318 macrophages.
319 To pinpoint when do the HSC-derived progenitors enter the thymus, we
320 devised two complementary experiments. First, we evaluated the contribution
321 of circulating adult monocytes to thymic macrophages without the
322 confounding effect of radiation damage on the thymus. We created shield
323 chimeras by subjecting CD45.1 mice to a lethal dose of irradiation while
324 protecting their upper body and the thymus with a 5 cm lead shield followed
325 by reconstitution with CD45.2 bone marrow (Fig. 3d). While the donor-derived
326 monocytes in the blood were, on average 20%, less than 2% of thymic
327 macrophages were $CD45.2^+$ (Fig. 3e and f), suggesting a relatively minor
328 (<10%) contribution of adult circulating monocytes to the thymic macrophage
329 pool consistent with a previous report[37]. Second, we transplanted E15.5
330 embryonic thymuses expressing GFP ubiquitously under the control of the
331 *ROSA26* locus (*ROSA26*^{GFP}) under the kidney capsule of adult mice and
332 analyzed them six weeks later (Fig. 3g). By that time, >99% of thymocytes
333 were derived from GFP^- host HSCs (Fig. 3h and i). As a positive control for
334 donor-derived cells, we used the thymic epithelial cells. The vast majority of
335 $EpCAM^+$ thymic epithelial cells (>90%) were still GFP^+. An identical
336 proportion of thymic macrophages was also GFP^+. The results from our

transplantation experiments show that the progenitors of almost all thymic macrophages are of embryonic origin. Altogether our results suggest that resident thymic macrophages are derived from multiple waves of progenitors. Initially, the thymus is settled by YS-derived progenitors that contribute substantially to the thymic macrophage pool during the embryonic period. In parallel with them, YS-independent progenitors infiltrate the thymus before E15.5 and establish themselves as the dominant population before birth. Adult HSC-derived monocytes contribute relatively little to the pool of thymic resident macrophages in young adult mice.

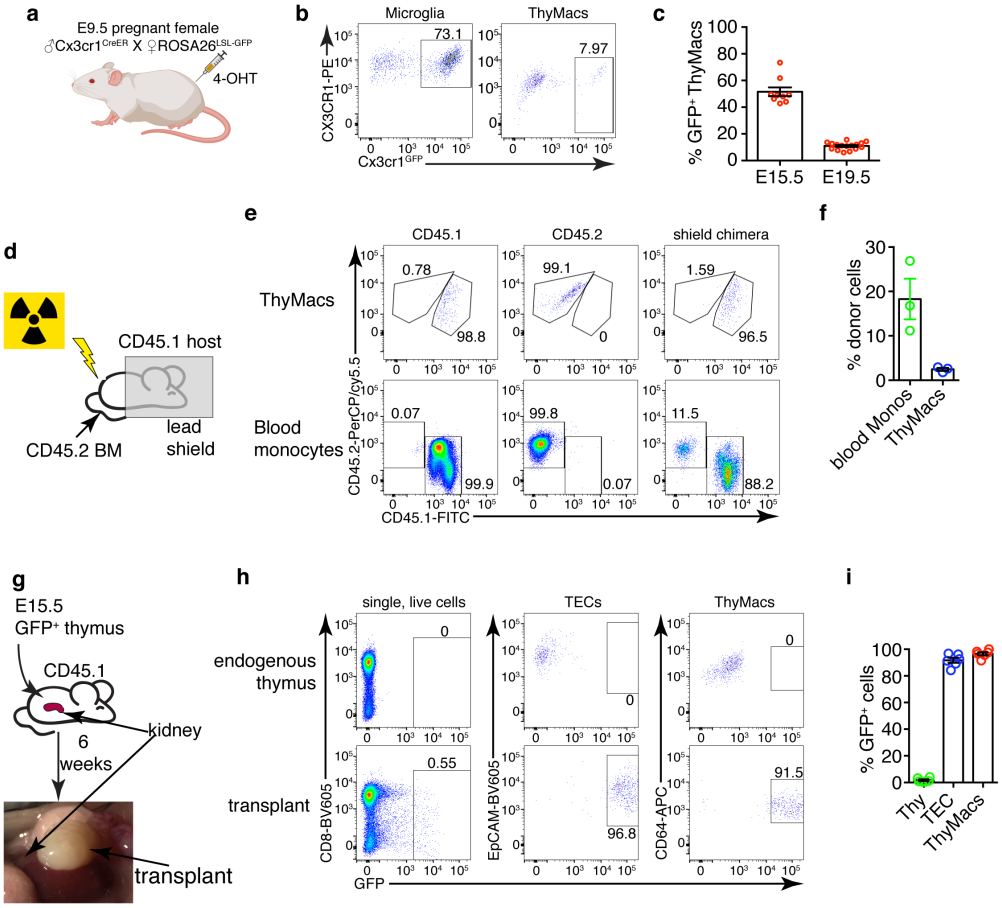

Figure 3. Yolk sac (YS)-derived and non-YS-derived embryonic progenitors sequentially contribute to the thymic macrophage pool. a Scheme of the YS-progenitor labeling experiments. E9.5 pregnant *ROSA26*$^{LSL\text{-}GFP}$ mice mated with *Cx3cr1*^{CreER} males were injected with 4-

350 hydroxytamoxifen (4-OHT) and sacrificed at E15.5 or E19.5. **b** Representative
351 flow cytometry plots of the *Cx3cr1*^{GFP} expression in microglia (CD45^{+}CD11b^{+}
352 cells in the brain) and ThyMacs of the pups. **c** Frequencies of GFP^{+} ThyMacs
353 at E15.5 and E19.5 adjusted to the degree of labeling of microglia. **d** Scheme
354 of the shield chimera experiments. Congenic CD45.1 mice were lethally
355 irradiated with their upper body protected by a 5 cm thick lead shield and then
356 injected with CD45.2^{+} bone marrow. **e** Representative flow cytometric
357 analysis of ThyMacs and CD115^{+}CD11b^{+} blood monocytes for donor-derived
358 (CD45.2^{+}) cells. Non-chimeric CD45.1 and CD45.2 samples serve as controls
359 for the gating. **f** Frequencies of donor-derived ThyMacs and blood
360 monocytes. **g** Scheme of the thymus transplantation experiments. **h**
361 Representative flow cytometry plots of GFP expression in thymocytes (Thy),
362 CD45^{-}EpCAM^{+} thymic epithelial cells (TECs), and thymic macrophages
363 (ThyMacs) six weeks after the transplantation. The host thymus (endogenous
364 thymus) serves as a negative control. The percentages of GFP^{+} cells are
365 indicated in the plots. **i** Frequencies of GFP^{+} cells in different cell populations
366 in the transplanted thymus. Data in **c**, **f**, and **i** are mean±SEM with two litters,
367 three, and five mice per group, respectively. The numbers in the flow
368 cytometry plots are the percent of cells in the respective gates. Each dot is an
369 individual mouse or embryo.
370

371 **Thymic macrophages can proliferate in situ**

372 The fact that macrophages can persist for many weeks in the thymus
373 without constant replacement from blood monocytes suggests that they can
374 divide in situ. Staining for the proliferation marker Ki-67 revealed that ~4% of

375 the cells expressed this marker compared to an isotype control (Fig. 4a and
376 b). To obtain further proof that thymic macrophages are proliferative, we
377 tested the incorporation of the nucleotide analog 5-Ethynyl-2'-deoxyuridine
378 (EdU). Short-term EdU labeling experiments unexpectedly revealed that
379 thymic macrophages become EdU^+ with faster kinetics than thymocytes (Fig.
380 4c). The most likely explanation for this puzzling result is that some of the
381 thymic macrophages have engulfed apoptotic thymocytes that have recently
382 divided and incorporated EdU. Thus, EdU could have accumulated in these
383 macrophages through phagocytosis and not through cell division. To
384 circumvent this caveat, we designed a pulse-chase experiment (Fig. 4d).
385 Mice were injected daily with EdU for 21 days so that all cells that proliferate
386 in that period would incorporate the label. The vast majority of thymocytes
387 and thymic macrophages became EdU^+ at d. 21 (Fig. 4e). After 21 more days
388 of "chase period", only ~0.2% of thymocytes had retained the EdU label,
389 consistent with the existence of a very small population of long-term resident
390 thymocytes consisting mainly of regulatory T cells and NKT cells[54] (Fig. 4e
391 and f). However, ~5% of the thymic macrophages were EdU^+, suggesting
392 they divided during the labeling period. Finally, we sorted thymic
393 macrophages and subjected them to cell cycle analysis. Although almost all
394 thymic macrophages were in G0/G1 phase, a small population of ~3% was in
395 G2/M phase of the cell cycle (Fig. 4g and h). Collectively, three independent
396 approaches documented that 3-5% of thymic macrophages are actively
397 dividing under homeostatic conditions within the thymus. These findings can
398 explain the long-term maintenance of these cells within the organ without a
399 constant influx of progenitors.

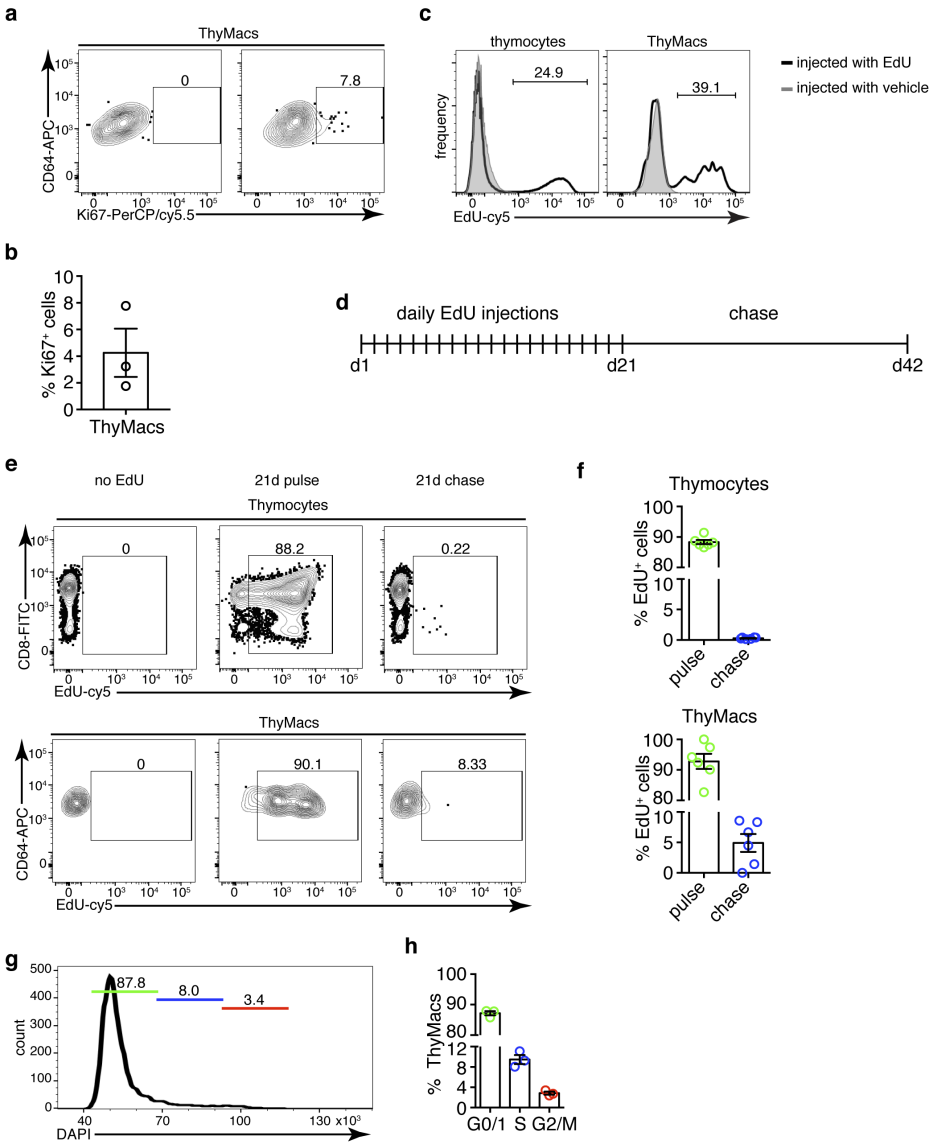

Figure 4. Thymic macrophages exhibit a low degree of proliferation. a Example flow cytometry plots of Ki67 staining of thymic macrophages (ThyMacs). **b** Frequency of Ki67^{+} thymic macrophages. **c** Example flow cytometry plots of the EdU accumulation in thymocytes and thymic macrophages 2 hours after 1 mg EdU i.p. or vehicle injection. The numbers inside flow plots are the percentage of EdU^{+} cells from mice injected with EdU. Data are representative of three independent experiments. **d** Scheme of EdU pulse/chase experiment: mice were injected daily with 1 mg EdU i.p for 21 days and then rested for 21 more days. **e** Example flow cytometry plots of

409 EdU staining of thymocytes (upper row) and ThyMacs (lower row). **f**
410 Frequencies of EdU$^+$ cells among thymocytes (top graph) and ThyMacs
411 (bottom graph). **g** Example flow cytometry plot of cell cycle analysis of FACS
412 sorted ThyMacs. **h** Frequencies of ThyMacs in different stages of the cell
413 cycle. The numbers in the flow cytometry plots are the percent of cells in the
414 respective gates. Data are mean±SEM from three mice (**b** and **h**) or 6-7
415 individual mice (**f**). Each dot is an individual mouse.
416

417 **Expression of *Timd4* and *Cx3cr1 can distinguish* two populations of**
418 **thymic macrophages**

419 To determine if thymic macrophages are heterogeneous, we turned to our
420 scRNA-Seq data. Once we zoomed onto *Mafb* expressing cells, we could
421 distinguish three separate populations: 1) monocytes that expressed high
422 levels of *Ly6c2* and *Itgam* (CD11b) but did not express *Mertk*; 2) *Timd4*$^+$
423 (encoding TIM4) macrophages that also expressed high levels of *Spic* and
424 *Slc40a1*, but low levels of *Cx3cr1*; 3) *Cx3cr1*$^+$ macrophages that expressed
425 low levels of *Timd4*, *Spic*, and *Slc40a1* (Fig. 5a and b). Both macrophages
426 and monocytes expressed *Fcgr1* (CD64). A minority of macrophages
427 expressed high levels of *Mki67*, indicating that they might be proliferating,
428 corroborating our earlier data. Interestingly, most of the *Mki67* expressing
429 macrophages belonged to the *Cx3cr1*$^+$ population.

430 We confirmed the results from scRNA-Seq by flow cytometry. We could
431 identify discrete TIM4$^+$*Cx3cr1*$^{GFP-}$ and TIM4$^-$*Cx3cr1*$^{GFP+}$ macrophages (Fig.
432 5c). There was even TIM4$^+$*Cx3cr1*$^{GFP+}$ intermediate population that could not
433 be distinguished in the scRNA-Seq dataset, likely because of the lack of

434 statistical power. To determine the localization of the two distinct macrophage
435 populations, we stained thymic sections from *Cx3cr1*^{GFP} mice with an antibody
436 to MerTK. The *Cx3cr1*$^{GFP-}$ MerTK^{+} cells correspond to *Timd4*$^{+}$ macrophages,
437 while the *Cx3cr1*$^{GFP+}$MerTK^{+} cells would be the *Cx3cr1*$^{GFP+}$ macrophages.
438 Strikingly, the two macrophage populations showed distinct localization.
439 *Timd4*$^{+}$ macrophages were located in the cortex, while the *Cx3cr1*$^{GFP+}$
440 macrophages resided in the medulla and the cortico-medullary junction (Fig.
441 5d).
442 To better understand the differences between the two populations of thymic
443 macrophages, we looked for differentially expressed genes. We included the
444 thymic monocytes in the comparison, as these cells clustered the closest to
445 macrophages. *Timd4*$^{+}$ macrophages expressed the highest levels of the
446 transcription factors *Spic*, *Maf*, and *Nr1h3*; the receptors for apoptotic cells
447 *Axl*, *Mertk*, and *Timd4*; and many Slc transporters such as *Slc40a1*, *Slc1a3*,
448 *Slco2b1*, *Slc11a1*, and *Slc7a7* (Fig. 5e and Table S2). *Cx3cr1*$^{+}$ macrophages
449 expressed high levels of the transcription factor *Runx3*; a distinct set of
450 phosphatidylserine receptors such as *Stab1*, *Anxa5*, and *Anxa3*; many
451 degradative enzymes such as *Mmp2*, *Mmp14*, *Dnase1l3*, *Acp5*, *Lyz2*, *Ctsz*,
452 *Ctss*, *Ctsd*, *Ctsl*; cytokines such as *Pdgfa*, *Cxcl16*, and *Ccl12*; and molecules
453 involved in MHC1 antigen presentation such as *B2m*, *H2-M2*, *H2-K1*, *H2-Q7*.
454 Thymic monocytes were characterized by differential expression of the typical
455 monocyte genes *Ly6c2*, *Ccr2*, and *S100a4*, and genes involved in MHC2
456 antigen presentation such as *Ciita*, *H2-DMb1*, *H2-Ab1*, and *Cd74*.
457

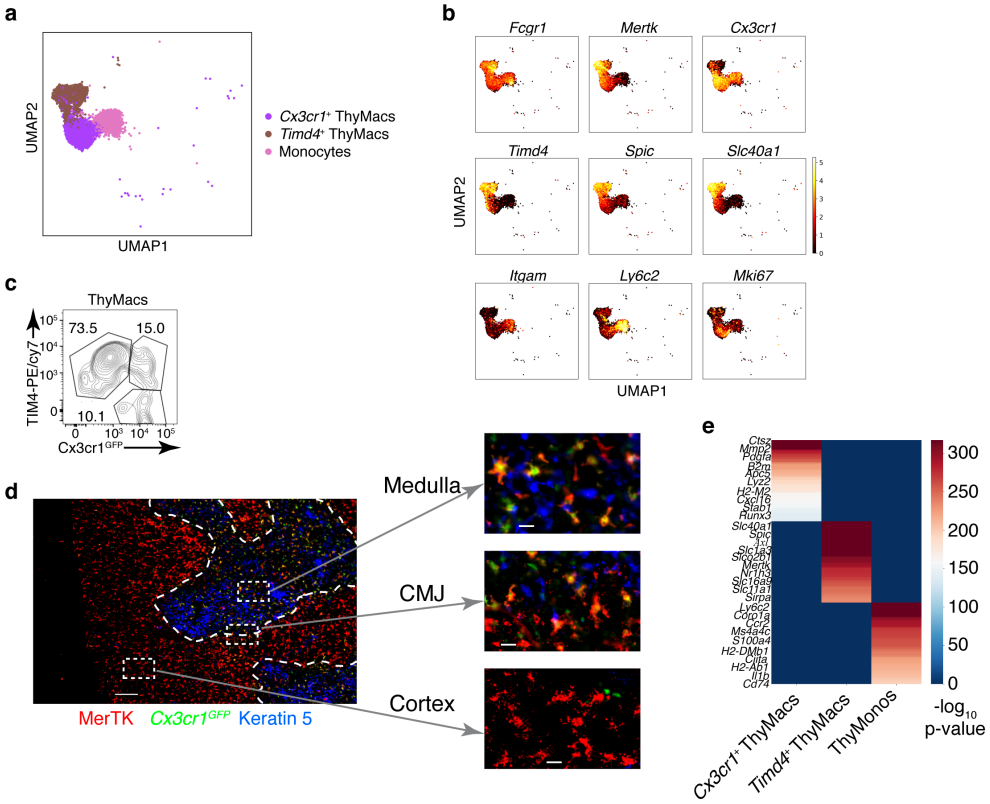

Figure 5: **Two populations of macrophages with distinct localization exist in the thymus. a** UMAP clusters from Fig. S2 with high expression of the transcription factor *Mafb* fall into three groups: monocytes, *Timd4*$^{+}$ macrophages, and *Cx3cr1*$^{+}$ macrophages. **b** Expression of the indicated genes in the three *Mafb*-positive clusters. **c** A flow cytometry plot of *Cx3cr1*^{GFP} and TIM4 expression in ThyMacs. The plot is representative of >10 individual experiments. The numbers inside the plot are the percentages of the cell populations in the respective gates. **d** Immunofluorescent staining of the thymus of *Cx3cr1*^{GFP} mouse stained with MerTK (a marker for all macrophages) and Keratin 5 (a marker for medulla). The scale bar is 150 μm. Areas in the cortex, medulla, and the cortico-medullary junction (CMJ) represented by the dashed boxes are enlarged below to show the co-localization of *Cx3cr11*^{GFP} and MerTK signal in CMJ and medulla, but not in cortex. The scale bars in the images below are 20 μm. The images are

472 representative of three individual mice. **e** Differentially expressed genes
473 among *Timd4*$^+$ thymic macrophages, *Cx3cr1*$^+$ thymic macrophages, and
474 thymic monocytes. The negative $\log_{10}$ p-values for the genes expressed in
475 each cluster were calculated as described in the Materials and Methods, and
476 the top 50 differentially expressed genes were plotted in the figure. Ten of
477 these genes are listed on the left.
478

479 ***Cx3cr1*$^+$ cells give rise to *Timd4*$^+$ cells during embryonic development**

480 To determine if the two populations of thymic macrophages are related, we
481 first analyzed the kinetics of their appearance during embryonic development.
482 At the earliest time point (E14.5), all thymic macrophages were *Cx3cr1*$^+$, and
483 only ~20% of them were also TIM4$^+$ (Fig. 6a and b). The proportion of TIM4$^+$
484 cells increased at E17.5, and TIM4$^+$*Cx3cr1*$^-$ cells started to appear. In the
485 neonatal period, almost all macrophages were TIM4$^+$, and very few remained
486 TIM4$^-$. The proportion of TIM4$^-$ cells increased in 6 weeks old mice, but TIM4$^+$
487 macrophages remained the dominant population. These kinetics (Fig. 6c) are
488 consistent with *Timd4*$^+$ macrophages developing from *Cx3cr1*$^+$ cells before
489 birth. Another plausible scenario is that distinct progenitors give rise to
490 different thymic macrophages populations (e.g., YS-progenitors give rise to
491 *Cx3cr1*$^+$*Timd4*$^-$ and HSC-derived progenitors develop into *Timd4*$^+$
492 macrophages). To test the latter hypothesis, we re-visited the fate mapping of
493 YS progenitors results (Fig. 3a). Although a larger part (~60% at E15.5) of
494 *Cx3cr1*$^+$TIM4$^-$ cells were derived from YS progenitors (Fig. 6d), a substantial
495 proportion (~40% at E15.5) of YS-derived TIM4$^+$ macrophages could clearly
496 be identified at both E15.5 and E19.5, suggesting that YS progenitors can

497 give rise to both *Cx3cr1*$^{+}$ and *Timd4*$^{+}$ cells. Extrapolating from the data, the
498 non-YS-derived progenitors (GFP^{-} cells) can also give rise to both *Timd4*$^{-}$ and
499 *Timd4*$^{+}$ cells. Thus, the simplest explanation for our findings is that *Timd4*$^{+}$
500 cells develop from *Cx3cr1*$^{+}$ cells during embryonic development. This
501 transition is complete in the first week after birth as there were essentially no
502 *Cx3cr1*$^{+}$ thymic macrophages remaining at d.7 (Fig. 6a and b).

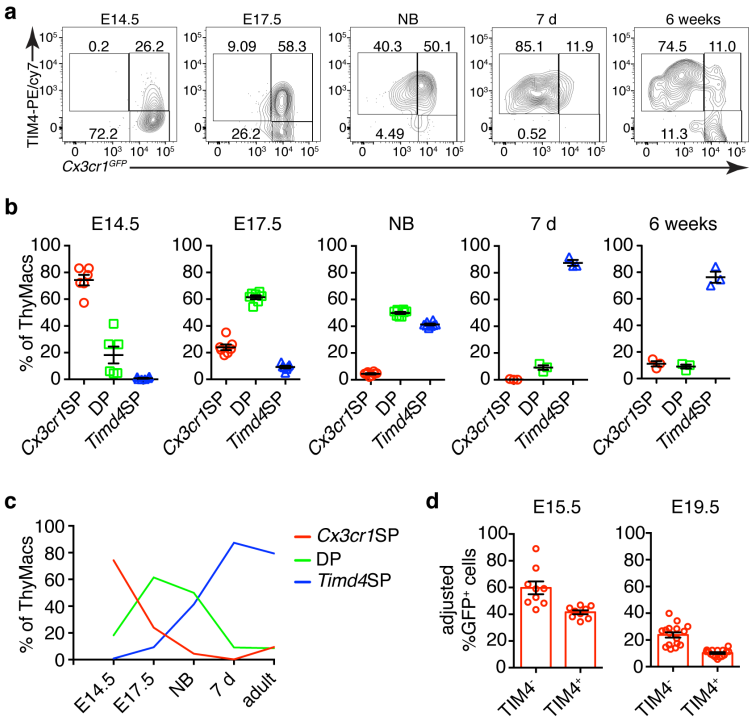

503

504 **Figure 6. *Timd4*$^{+}$ thymic macrophages are derived from *Cx3cr1*$^{+}$ cells**
505 **during embryonic development. a** Example flow cytometry plots for the
506 expression of *Cx3cr1*^{GFP} and TIM4 on thymic macrophages at different times
507 during embryonic development (E14.5, E17.5), immediately after birth, at 7
508 days, and 6 weeks of age. **b** Frequencies of *Timd4*$^{+}$*Cx3cr1*$^{-}$ (*Timd4* single-
509 positive or *Timd4*SP), *Timd4*$^{+}$*Cx3cr1*$^{+}$(double-positive or DP), and
510 *Cx3cr1*$^{+}$*Timd4*$^{-}$ (*Cx3cr1* single-positive or *Cx3cr1*SP) thymic macrophages at
511 the indicated time points. **c** Kinetics of the changes in different subpopulations
512 of thymic macrophages from E14.5 to 6 weeks. **d** Frequencies at E15.5 and

513 E19.5 of GFP-labeled cells among *TIM4*$^{+}$ or *TIM4*$^{-}$ cells in *Cx3cr1*^{CreER} X
514 *ROSA26*$^{LSL\text{-}GFP}$ embryos treated with 4-OHT at E9.5. Data is from at least two
515 independent experiments for each panel. Each symbol is an individual mouse
516 or embryo.
517
518 ***Timd4*$^{+}$ thymic macrophages self-maintain, while *Cx3cr1*$^{+}$ cells slowly**
519 **accumulate with age**
520 To understand how are the resident thymic macrophage populations
521 maintained during adult life, we induced recombination in *Cx3cr1*^{CreER} X
522 *ROSA26*$^{LSL\text{-}GFP}$ mice during the neonatal period (Fig. 7a) or at 6 weeks of age
523 (Fig. 7c) and compared the proportion of GFP^{+} cells 3 and 42 days after
524 labeling. The extent of labeling of *Timd4*$^{+}$ thymic macrophages did not
525 change within these 6 weeks, no matter whether the mice were treated with
526 Tamoxifen in the first week after birth or at 6 weeks (Fig. 7b and d),
527 suggesting steady-state maintenance and absence of a significant influx from
528 unlabeled cells (e.g., monocytes). In contrast, the proportion of labeled
529 *Timd4*$^{-}$ thymic macrophages decreased significantly 6 weeks after Tamoxifen
530 injection in both neonatal and adult mice, suggesting that this population was
531 being diluted by unlabeled cells. To further substantiate these findings, we
532 examined older WT mice and found out that the proportions of *Timd4*$^{-}$ thymic
533 macrophages increased with age, and in mice >8 months old, they accounted
534 for ~70% of all macrophages in the organ (Fig. 7e). Thus, we conclude that
535 *Timd4*$^{+}$ macrophages can maintain themselves for long periods in the cortex
536 of the thymus, Since the first week of life, *Cx3cr1*$^{+}$ cells are slowly being
537 recruited to the medulla and cortico-medullary junction, and in aging mice

538 form the predominant phagocytic population in the organ.

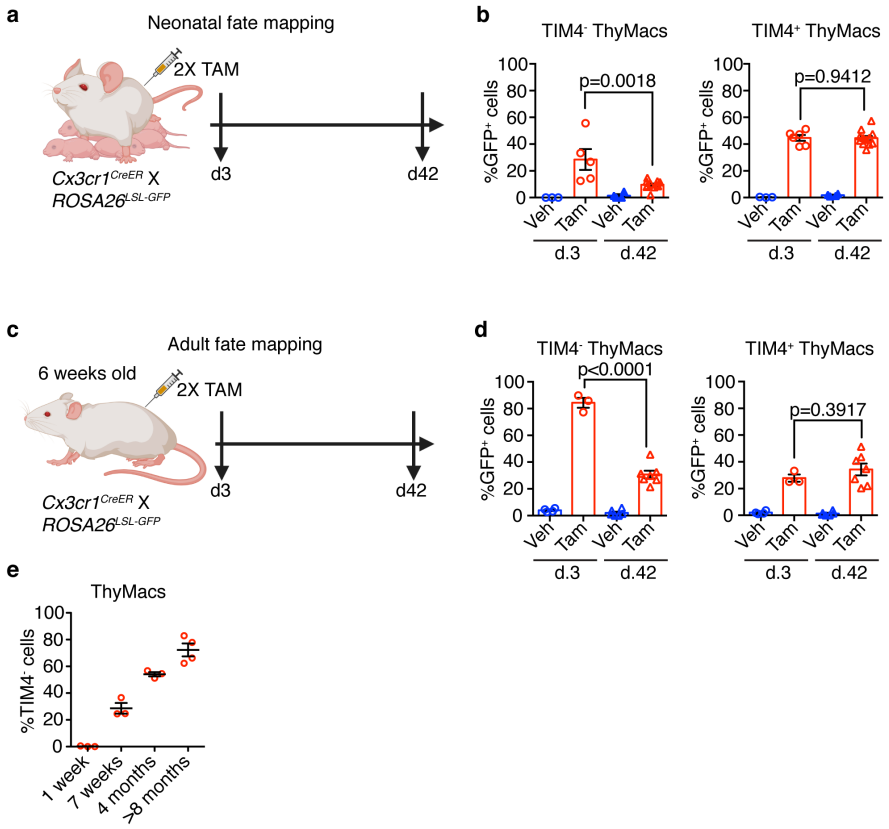

539

540 **Figure 7. *Timd4*⁺ thymic macrophages self-maintain during adult life,**
541 **while *Cx3cr1*⁺ cells slowly accumulate with age. a** Scheme of the neonatal
542 fate mapping: A nursing dam was injected twice with Tamoxifen (Tam) or
543 vehicle (Veh) in the first week after giving birth to *Cx3cr1*^{CreER} X *ROSA26*$^{LSL-}$
544 ^{GFP} pups. Three or 42 days after the last injection, the pups were sacrificed,
545 and the degree of labeling of *Timd4*⁺ and *Timd4*⁻ thymic macrophages was
546 examined by flow cytometry. **b** Frequencies of GFP⁺ *Timd4*⁺ or *Timd4*⁻ thymic
547 macrophages from neonatally fate mapped mice after 3 and 42 days. Vehicle
548 injected nursing dam litters (Veh) served as a control for non-specific labeling.
549 **c** Scheme of the adult fate mapping: Six weeks old *Cx3cr1*^{CreER} X *ROSA26*$^{LSL-}$
550 ^{GFP} mice were injected twice with Tamoxifen (Tam) or vehicle (Veh). Three or
551 42 days after the last injection, the mice were sacrificed, and the degree of
552 labeling of *Timd4*⁺ and *Timd4*⁻ thymic macrophages was examined by flow

553 cytometry. **d** Frequencies of GFP$^+$ *Timd4*$^+$ or *Timd4*$^-$ thymic macrophages
554 from adult fate mapped mice after 3 and 42 days. **e** Frequencies of TIM4$^-$
555 thymic macrophages at different ages. The data is mean±SEM from 2
556 independent experiments (**b**) or at least 3 individual mice per time point (**d** and
557 **e**). Each symbol is an individual mouse. Statistical significance was
558 determined with unpaired Student's t-test.
559

560 **Discussion**

561 Here, we have described the phenotype, transcriptional profile, localization,
562 diversity, ontogeny, and maintenance of macrophages in the thymus. These
563 cells express the typical macrophage markers CD64, MerTK, and F4/80 and
564 are transcriptionally most similar to splenic red pulp macrophages and liver
565 Kupffer cells. However, they have a unique expression profile dominated by
566 genes involved in antigen presentation and lysosomal degradation. We found
567 that thymic macrophages consist of two populations with distinct localization.
568 *Timd4*$^+$ macrophages occupied the cortex, while *Cx3cr1*$^+$ cells were located in
569 the medulla and the cortico-medullary junction. While YS-derived
570 macrophages dominated the early stages of thymus development, they were
571 quickly replaced by non-YS embryonic progenitors that gave rise to the
572 *Timd4*$^+$ thymic macrophages that could proliferate and self-maintain. *Cx3cr1*$^+$
573 macrophages started slowly accumulating after birth and in old mice became
574 the most abundant population.

575 Altogether our data depict thymic macrophages as typical tissue-resident
576 macrophages with origin from multiple hematopoietic waves, ability to self-
577 maintain, and expression of the core macrophage-specific genes. They were

578 most similar transcriptionally to splenic red pulp macrophages and Kupffer
579 cells, which is not surprising considering that they all specialize in
580 efferocytosis and have efficient lysosomal degradation machinery. These
581 three populations also shared expression of the transcription factor *Spic* that
582 is induced by heme released following red blood cells phagocytosis[52].
583 However, the thymus is not known as a place for erythrocyte degradation.
584 Thus the mechanism for *Spic* up-regulation in thymic macrophages is unclear.
585 The unique features of thymic macrophages include high expression of
586 genes involved in the IFN-I pathway, antigen presentation, and lysosomal
587 degradation. The up-regulation of IFN-I-stimulated genes such as *Stat1*,
588 *Stat2*, *Irf7*, and *Irf8* can be explained by the constitutive secretion of IFN-I by
589 thymic epithelial cells[55,56]. The purpose of IFN-I expression in the thymus
590 in the absence of a viral infection is unclear. Still one possibility is that it
591 mediates negative selection to IFN-dependent genes as part of central
592 tolerance.
593 Thymic macrophages highly express molecules involved in antigen
594 presentation, including MHC1 and MHC2, although the latter is expressed at
595 lower levels than in cDCs. Thus, they have the potential to present antigens
596 for both negative selection and agonist selection. These two activities have
597 traditionally been assigned solely to cDCs[57]. However, recent evidence
598 suggests that negative selection is most efficient when the cell that presents
599 the antigen to auto-reactive thymocytes is also the one that phagocytoses
600 it[58]. So, macrophages participation in thymocyte selection needs to be re-
601 evaluated with optimized isolation procedures and specific genetic tools.

602 The extraordinary ability of thymic macrophages to engulf and degrade
603 apoptotic thymocytes has been appreciated for a long time[31], and our RNA-
604 Seq data provides additional supporting evidence for this function by
605 highlighting the up-regulation of pathways involved in lysosomal degradation.
606 An interesting topic for future research would be to understand how the
607 metabolites derived from apoptotic cells are returned to the microenvironment
608 to support the proliferation of immature thymocytes. A *SoLute Carrier* (*Slc*)
609 genes-based program has been described in vitro[59], but its relevance to
610 tissue-resident macrophages remains to be determined. Altogether, our study
611 demonstrates that thymic macrophages are a unique subset of tissue-resident
612 macrophages and support the idea that resident macrophage phenotype is
613 determined by the combination of ontogeny, microenvironment, and other
614 factors[60].
615 Together with the study by Tacke et al., our work builds the following model
616 for thymic macrophage origin[37]: Thymic macrophages develop in three
617 distinct waves: YS-derived progenitors dominate the early stages of thymus
618 development but are replaced before birth by a second wave of YS-
619 independent embryonic progenitors that forms the bulk of thymic
620 macrophages after birth and can self-maintain into adulthood. With age, there
621 is a slow and steady influx of *Timd4*$^{-}$*Cx3cr1*$^{+}$ macrophage precursors that
622 occupy the medulla and cortico-medullary junction, becoming the major
623 phagocytic population in the thymus of older mice (>8 months). The second
624 wave of YS-independent macrophages is most likely the progeny of
625 embryonic HSCs based on *Flt3*^{Cre} fate mapping that showed that >80% of
626 thymic macrophages in adult mice are descendants of HSCs[37]. Whether

627 HSC-independent fetal liver monocytes contribute to thymic macrophages and
628 to what extend awaits the creation of models that can specifically target this
629 population of progenitors. Recruitment of circulating monocytes to the resident
630 macrophage pool in the thymus has been ruled out previously by parabiosis
631 and *Ccr2*$^{-/-}$ mice[37]. Our shield chimera experiments have arrived at similar
632 conclusions. However, the relatively short duration of these experiments and
633 their focus on the bulk thymic macrophages have prevented the recognition of
634 the gradual accumulation of *Timd4*$^{-}$ macrophages. Once we zoomed in on this
635 minor cell population in young mice, the fate mapping clearly showed an influx
636 of unlabeled progenitors. Whether the progenitors of *Timd4*$^{-}$ macrophages
637 are monocytes remains to be formally demonstrated. However, in all
638 macrophage populations exhibiting replacement in adults examined to date,
639 monocytes have been singled out as the source[12,19,22,24,25,30]. An
640 alternative possibility involves thymocyte progenitors that under certain
641 circumstances have been shown to differentiate into macrophages and
642 granulocytes in the thymus[42,43]. However, if this occurs in unmanipulated
643 mice at a steady-state remains unclear.
644 The strict spatial segregation of the two macrophage populations in the
645 thymus implies that they might have distinct functions. *Timd4*$^{+}$ cells are
646 restricted to the cortex and are particularly abundant in the deeper cortex,
647 close to the medulla. Both positive and negative selection of thymocytes occur
648 there, so we speculate that *Timd4*$^{+}$ macrophages might be specialized in
649 efferocytosis of CD4^{+}CD8^{+} (double-positive) thymocytes that cannot interact
650 with cortical thymic epithelial cells and die by neglect or are auto-reactive and
651 undergo clonal deletion in the cortex[61]. On the other hand, *Cx3cr1*$^{+}$

652 macrophages accumulate in the medulla; the thymic region specialized in
653 negative selection to tissue-restricted antigens (TRA). They might contribute
654 to the process in several ways: 1) by carrying TRAs from blood and peripheral
655 organs. A similar process has been described for cDC2 (SIRPα^+ DCs)[62]. In
656 fact, *Cx3cr1*$^+$ thymic macrophages could have contributed to this role because
657 they were not distinguished from cDC2 in this study. 2) By capturing TRAs
658 from *Aire*$^+$ medullary thymic epithelial cells and presenting them to auto-
659 reactive thymocytes as shown for DCs[63-65]. 3) By phagocytosing apoptotic
660 TRA-specific medullary thymocytes, a process we have observed before[58].
661 The exact involvement of thymic macrophages in the selection events in the
662 thymus remains to be determined.
663 The accumulation of the *Cx3cr1*$^+$ cells in older mice has clear implications
664 for thymus aging. One key feature of thymus involution is the accumulation of
665 extracellular matrix produced by fibroblasts and the emergence of white
666 adipocytes[66]. The *Cx3cr1*$^+$ subset is the predominant producer of the growth
667 factor PDGFα that is required for the maintenance of adipocyte stem cells and
668 can stimulate tissue fibrosis[67,68]. The gradual accumulation of *Cx3cr1*$^+$
669 macrophages could increase the availability PDGFα in the aging thymus
670 stimulating extracellular matrix production and differentiation of precursors
671 into adipocytes. This model predicts that limiting the influx of *Cx3cr1*$^+$
672 macrophage precursors could delay thymus involution.
673 Recent work described a novel phagocytic and antigen-presenting cell type
674 in the thymus called monocyte-derived DCs[65]. The phenotype of these cells
675 overlaps with the CD64$^+$F4/80^{lo}CD11b$^+$ cells in our study. However, we favor
676 the classification of these cells as monocytes based on their expression of

677 *Mafb*, CD64, and Ly6C (Fig. 5b) and lack of expression of the defining DC
678 transcription factor *Zbtb46* (Fig. S2c)[69]. As monocytes can differentiate into
679 cDC2, particularly in the context of inflammation[70], the precise identity and
680 the relationship of this population to thymic cDC2 remain to be established.
681 In the past several years, scRNA-Seq has come to the forefront of
682 biologists' efforts to disentangle the cellular diversity of tissues. Several
683 comprehensive studies have included samples from mouse or human
684 thymus[71-73]. However, in these studies, too few thymic macrophages were
685 sampled to give meaningful clustering results. Efforts specifically targeting
686 the thymus have provided considerably more information[74,75], but
687 macrophage diversity was still not recognized. Characterization of rare
688 populations such as thymic macrophages (~0.1% of all cells in the thymus)
689 requires optimized enzymatic digestion procedures and enrichment strategies,
690 as has been demonstrated already for thymic epithelial cells[76,77]. Our
691 scRNA-Seq dataset provides a rich resource for the unbiased characterization
692 of myeloid cells in the thymus and will greatly aid in the understanding of the
693 myeloid landscape of the thymus.
694 In summary, our work comprehensively characterizes macrophages in the
695 thymus and paves the way for exploration of their functions.
696

697 **Materials and methods**

698 **Mice**

699 C57BL/6Narl (CD45.2) mice were purchased from the National Laboratory
700 Animal Center, Taipei, Taiwan. MAFIA (MAcrophage Fas-Induced Apoptosis)
701 [78], *Cx3cr1*^{GFP} [79], *Spic*^{GFP} [52], *Cx3cr1*^{CreER} [53], and *B6.SJL-Ptprca*

702 *Pepcb/BoyJ* (CD45.1) mice were purchased from the Jackson Laboratories.
703 *Cd11c*^{YFP} [80] and *Lyz2*^{GFP} [81] mice have been described. Mice ubiquitously
704 expressing GFP from the *ROSA26* locus were generated by breeding
705 *Pdgfra*^{Cre} [82] and *ROSA26*$^{LSL\text{-}ZsGreen}$ (also known as *ROSA26*$^{LSL\text{-}GFP}$ or Ai6)
706 mice[83] (both from the Jackson Laboratories). A mouse from this cross was
707 identified, in which the STOP cassette was deleted in the germline. It was
708 designated *ROSA26*^{GFP} and subsequently bred to C57BL/6 mice. All mice
709 were used at 4-10 weeks of age unless otherwise specified. Mice were bred
710 and maintained under specific pathogen-free conditions at the animal facility
711 of National Yang-Ming University. All experimental procedures were approved
712 by the Institutional Animal Care and Use Committee (IACUC) of National
713 Yang-Ming University.
714
715 **Treatment with 5-Ethynyl-2'-deoxyuridine (EdU)**
716 Mice were i.p. injected with 1 mg EdU (Carbosynth) dissolved in PBS daily
717 for 21 days and then rested for 21 more days. Cells from the thymus were
718 harvested on day 21 or 42. In some experiments, the mice were sacrificed 2
719 hours after the first EdU injection.
720
721 **Shield chimera generation**
722 CD45.1 mice were anesthetized by i.p. injection of 120 μg/g body weight
723 Ketamine hydrochloride (Toronto Research Chemicals) and 12 μg/g body
724 weight Xylazine hydrochloride (Sigma). Anesthetized mice were taped to a 5
725 cm thick lead block so that the lead block covered the head and the chest
726 down to the bottom of the rib cage. Then, they were irradiated with a lethal

727 dose (1000 rad) from a ^{137}Cs source (Minishot II, AXR) so that only their
728 abdomen and hind legs were exposed. After recovery from anesthesia, the
729 mice were transfused i.v. with 10^7 bone marrow cells from a congenic
730 (CD45.2) donor. Then, they were given Trimerin (0.5 mg/mL Sulfadiazine +
731 0.1 mg/mL Trimethoprim, China Chemical and Pharmaceutical Co., Tainan,
732 Taiwan) in the drinking water for the first two weeks after the irradiation and
733 analyzed after six weeks.
734
735 **Cell isolation from thymus, blood, and peritoneal cavity**
736 Thymocytes were obtained by mechanical disruption of the thymus with a
737 syringe plunger. For myeloid cell isolation, mouse thymuses were cut into
738 small pieces and digested with 0.2 mg/mL DNase I (Roche) and 0.2 mg/mL
739 collagenase P (Roche) in complete DMEM for 20 min at 37˚C with frequent
740 agitation. 1.6 mg/mL Dispase I (ThermoFisher) was added to the enzymatic
741 mixture for thymic epithelial cell isolation. In some experiments, thymic
742 myeloid cells and thymic epithelial cells were enriched by 57% Percoll PLUS
743 (GE Healthcare) discontinuous gradient centrifugation at 4˚C, 1800 rpm, for
744 20 min without brake. Cells at the interface were collected and washed with
745 PBS to remove residual silica particles. Then the cells were resuspended in
746 PBS with 0.5% BSA (HM Biological), filtered through a 70 μm filter, and kept
747 on ice.
748
749 Blood was isolated by cardiac puncture of sacrificed mice and immediately
750 diluted with PBS. After centrifugation, the cell suspensions were treated with
751 ammonium chloride-potassium lysis buffer for 3 min on ice once or twice.

752 Peritoneal cavity cells were obtained by lavage with 5 mL PBS + 2 mM EDTA
753 (Merck). Following gentle massage, the cavity was opened with an abdominal
754 incision, and lavage fluid was collected.
755
756 **Flow cytometry**
757 Single-cell suspensions (0.5 – 2X10^6 cells) from thymus, blood, or
758 peritoneal cavity were blocked with supernatant from 2.4G2 hybridoma (a kind
759 gift by Dr. Fang Liao, Academia Sinica, Taipei, Taiwan) and stained with
760 fluorochrome- or biotin-labeled antibodies for 20 min on ice in PBS + 0.5%
761 BSA + 2 mM EDTA + 0.1% NaN_3 (FACS buffer). The following antibodies
762 were used: CD11b (clone M1/70), MHC2 (M5/114.15.2), CD11c (N418),
763 F4/80 (BM8), CD115 (AFS98), SIRPα (P84), CD45 (30-F11), NK1.1 (PK136),
764 TIM4 (RMT4-54), Gr-1 (RB6-8C5), CD64 (X54-5/7.1), Siglec H (551), Ly6C
765 (HK1.4), CD3ε (145-2C11), CD8α (53-6.7), CD19 (6D5), B220 (RA3-6B2),
766 CD4 (GK1.5), CD51 (RMV-7), CD45.1 (A20), CD45.2 (104), CX3CR1
767 (SA011F11), and EpCAM (G8.8) from BioLegend; Axl (MAXL8DS), MerTK
768 (DS5MMER), and Ki67 (SolA15) were from eBioscience; Siglec F (E50-2440),
769 CD90.2 (30-H12), and CD11c (HL3) were from BD Biosciences. Cells were
770 washed, and if necessary, incubated for 20 more min with fluorochrome-
771 labeled Streptavidin: Streptavidin-AF647 (Jackson Immunoresearch) or
772 Streptavidin-APC/cy7, Streptavidin-BV421, Streptavidin-BV605 (BioLegend).
773 After the last wash, the cells were resuspended in FACS buffer containing
774 DAPI (BioLegend), Propidium Iodide (Sigma), or DRAQ7 (BioLegend) and
775 analyzed immediately on an LSR Fortessa flow cytometer running Diva 8

776 software (BD Biosciences). Typically, 500,000 cells were collected from
777 thymus samples. Data were analyzed using FlowJo software (TreeStar).
778
779 For intracellular staining, after surface antibody staining, the cells were
780 labeled with Zombie Aqua (BioLegend) for 30 min in ice. Then, the cells were
781 fixed with 2% paraformaldehyde (Electron Microscope Sciences) in PBS for
782 20 min on ice, permeabilized with either 0.5% Triton-X 100 (Sigma) for 20 min
783 on ice, or with Foxp3 staining kit (eBioscience) according to the protocol
784 provided by the manufacturer, and stained with antibodies for intracellular
785 markers for 40-60 min on ice.
786
787 For cell cycle analysis, 1-5X10^5 sorted thymic macrophages were fixed with
788 70% ethanol for 2 h on ice. The cells were spun down at 1800 rpm for 20 min
789 at 4˚C, washed with PBS, and stained with 1 μg/ml DAPI (BioLegend) for 30
790 min at room temperature in the dark.
791
792 For EdU staining, after surface marker and Zombie Aqua staining, cells
793 were fixed with 2% paraformaldehyde in PBS for 20 min on ice and
794 permeabilized with 0.5% Triton X-100 in PBS at room temperature for 20 min.
795 EdU was detected by adding an equal volume of 2X Click reaction buffer
796 consisting of 200 mM Tris, 200 mM ascorbic acid (Acros), 8 mM $CuSO_4$
797 (Acros), 8 μM Cy5-azide (Lumiprobe) to the permeabilized cells resuspended
798 in 0.5% Triton X-100 in PBS and incubation at room temperature for 30 min.
799 Cells were washed twice with 0.5% Triton X-100 in PBS and analyzed on a
800 flow cytometer.

801

802 **Cell sorting**

803 The sorting of thymic macrophages was done following the IMMGEN
804 guidelines. Briefly, the thymuses of 3 male C57BL/6Narl mice were harvested
805 in ice-cold staining buffer containing phenol red-free DMEM (Gibco) with 10
806 mM HEPES (Sigma), 0.1% NaN_3, and 2% FBS (Gibco). Single-cell
807 suspensions were prepared as described in the Flow cytometry section.
808 Percoll PLUS was used to enrich mononuclear cells. The cells were
809 resuspended at 10^8/mL in staining buffer and labeled with appropriate
810 antibodies for 15 min in ice. To sort thymic macrophages, the cells were first
811 labeled with biotinylated antibodies to lineage markers (Lin) – CD3, CD8, Gr1,
812 B220. After washing, the cells were stained with antibodies to CD11b, F4/80,
813 CD45, CD64, and Streptavidin-APC/cy7 for 15 min in ice. For sorting thymus
814 $XCR1^+$ and $SIRP\alpha^+$ cDCs, antibodies to XCR1, SIRPα, CD11c, MHC2, CD64,
815 and F4/80 were used. For sorting peritoneal cavity macrophages, antibodies
816 to ICAM2 and F4/80 were used. Immediately before sorting, the dead cells
817 were excluded with DRAQ7 or PI. For RNA Sequencing experiments, the
818 cells were double-sorted on FACS Melody, or Aria cell sorters (BD
819 Biosciences) and 1000 cells were directly deposited in TCL buffer (Qiagen),
820 frozen in dry ice and sent to IMMGEN for RNA sequencing. Four biological
821 replicates were prepared. For cytospin and cell cycle analysis, 1-5X10^5 cells
822 sorted on FACS Melody were collected in staining buffer.

823

824 **Cytospin**

825 Sorted cells were mounted on Superfrost PLUS slides (Thermo Scientific)
826 using a Cytospin centrifuge (Cytospin 3, Shandon) for 5 min at 500 rpm. Cells
827 were fixed with 2% paraformaldehyde for 10 min at room temperature and
828 stained with the Hemacolor Rapid Staining Kit (Merck Millipore). Images were
829 collected on BX61 upright microscope (Olympus) using 100X objective with
830 immersion oil and captured with a CCD camera. Images were then analyzed
831 and processed with ImageJ (NIH) and Adobe Photoshop 5.5 (Adobe).
832
833 **RNA sequencing analysis**
834 RNA sequencing was done at IMMGEN using Smart-seq2 protocol[84,85]
835 on a NextSeq500 sequencer (Illumina). Following sequencing, raw reads
836 were aligned with STAR to the mouse genome assembly mm10 and assigned
837 to specific genes using the GENCODE vM12 annotation. Gene expression
838 was normalized by DESeq2[86] and visualized by Morpheus
839 (https://software.broadinstitute.org/morpheus). Hierarchical clustering was
840 done with Cluster 3.0 and visualized with Java TreeView. Only genes with
841 SD>20 were used (10602 genes). The metric used was Pearson correlation
842 (uncentered), and the clustering method was average linking. Gene
843 expression of mouse transcription factors[87] was visualized in MultiplotStudio
844 of GenePattern[88]. GO enrichment was calculated and visualized in R by
845 using clusterProfiler[89].
846
847 **Timed pregnancies and embryonic thymus analysis**
848 To set up timed pregnancies, each male mouse (*Cx3cr1*$^{CreER/CreER}$,
849 *Cx3cr1*$^{GFP/GFP}$ or C57BL/6) and female mouse (*ROSA26*$^{LSL\text{-}GFP/LSL\text{-}GFP}$ or

850 C57BL/6) were housed together in the same cage for one night and separated
851 on the next day, which we defined as embryonic day 0.5 (E0.5). Female mice
852 were assumed to be pregnant if their weight gain was over 2 g at E8.5[90].
853 Thymuses from E14.5 and E17.5 embryos, neonatal, 1-weeks-old pups, and
854 adult mice (older than 6-weeks-old) were harvested, mechanically dissociated
855 with plastic sticks in 1.5-mL centrifuge tubes, and enzymatically digested with
856 0.2 mg/mL DNase I and 0.2 mg/mL collagenase P in complete DMEM for 20
857 min at 37˚C with frequent agitation. The cells were resuspended in PBS with
858 0.5% BSA, filtered through a 70 μm filter, kept on ice, and used flow
859 cytometric analysis as described in the Flow Cytometry section.
860

861 **Genetic fate mapping – E9.5, neonatal and adult**

862 For genetic fate mapping, timed pregnancies of *Cx3cr1*$^{CreER/CreER}$ male and
863 *ROSA26*$^{LSL\text{-}GFP/LSL\text{-}GFP}$ female mice were set up as described. To label the
864 *Cx3cr1*$^{+}$ erythromyeloid progenitors derived from embryonic yolk sac[8], 4-
865 hydroxytamoxifen (4-OHT from Sigma) was administered i.p. to pregnant
866 females on E9.5 at a dose of 75 μg/g (body weight). To improve the survival
867 of embryos and reduce the risk of abortions, Progesterone (Sigma) was co-
868 injected at a dose of 37.5 μg/g (body weight)[91]. To label the *Cx3cr1*$^{+}$ thymic
869 macrophages in *Cx3cr1*^{CreER} X *ROSA26*$^{LSL\text{-}GFP}$ neonates and adult mice,
870 Tamoxifen (TAM from Sigma) was injected i.p. at a dose of 2 mg/mouse to
871 lactating dams on postnatal day 3 and 4 (P3 and P4) or to adult mice for 2
872 consecutive days. Thymuses were harvested and analyzed 3 days or 6
873 weeks after the last injection by flow cytometry.
874

875 **scRNA-Seq – sorting, library generation, and sequencing**

876 scRNA-Seq was performed at the Genomics Center for Clinical and
877 Biotechnological Applications of NCFB (NYCU, Taipei, Taiwan). Briefly, the
878 thymuses of one female MAFIA and 2 male *Cd11c*^{YFP} mice were harvested
879 and enzymatically digested as described previously. Mononuclear cells were
880 enriched by 57% Percoll PLUS discontinuous centrifugation, washed to
881 remove silica particles, and resuspended at 10^6/mL in PBS with 0.04% BSA.
882 The cell suspensions were filtered through Falcon 35 μm strainer (Corning)
883 and stained with viability dye (PI or DAPI) immediately before sorting. Cell
884 sorting was performed on a FACS Melody sorter (BD Biosciences) running
885 FACS Chorus (BD Biosciences) software in purity mode. $3X10^5$ GFP or YFP
886 positive cells under the live/singlet gating were collected into 5 ml round
887 bottom tubes pre-coated with 0.04% BSA in PBS. Sorted cells were washed
888 and resuspended in 300 μL PBS with 0.04% BSA and then filtered again into
889 1.5-mL DNA LoBind tubes (Eppendorf) through a 35 μm strainer. The viability
890 of the cells was evaluated by Countess II (Invitrogen) and Trypan Blue
891 (ThermoFisher), and samples with cell viability rates higher than 85% were
892 used for encapsulation and library preparation. Single-cell encapsulation and
893 library preparation were performed using Single Cell 3' v3/v3.1 Gene
894 Expression solution (10x Genomics). All the libraries were processed
895 according to the manufacturer's instruction and sequenced on NovaSeq 6000
896 (Illumina) platform at the NHRI (Zhubei, Taiwan). Post-processing and quality
897 control were performed by the NYCU Genome Center using the CellRanger
898 package (v. 3.0.2, 10x Genomics). Reads were aligned to mm10 reference
899 assembly. Primary assessment with CellRanger reported 9,973 cell-barcodes

900 with 11,385 median unique molecular identifiers (UMIs, transcripts) per cell
901 and 3,076 median genes per cell sequenced to 71.0% sequencing saturation
902 with 94,260 mean reads per cell for MAFIA mouse sample; 9,801 cell-
903 barcodes with 13,467 median UMIs per cell and 3,211 median genes per cell
904 sequenced to 74.9% sequencing saturation with 119,820 mean reads per cell
905 for the first *Cd11c*^{YFP} mouse sample; 12,938 cell-barcodes with 14,439
906 median UMIs per cell and 3,199 median genes per cell sequenced to 71.4%
907 sequencing saturation with 108,585 mean reads per cell for the second
908 *Cd11c*^{YFP} mouse sample.
909
910 **Analysis of scRNA-Seq**
911 Preprocessing
912 The Scanpy[92] pipeline was used to read the count matrix. Three batches
913 of samples (one from GFP^{+} cells from MAFIA mouse and two from YFP^{+} cells
914 from *Cd11c*^{YFP} mice) were preprocessed independently and integrated later.
915 Cells that expressed <200 genes and genes that were expressed in <3 cells
916 were filtered out. The percentage of mitochondrial genes was calculated -and
917 cells with >10% mitochondrial genes were removed. Cells with >7,000 genes
918 or <1,000 genes were also removed. Read counts were normalized to library
919 size 10,000 and log-transformed with scanpy.pp.log1p function.
920 Datasets integration and batch effect correction
921 Read count matrices and spliced/unspliced matrices were merged first.
922 Principal Component Analysis was applied to reduce dimensions to 70.
923 BBKNN[93] was then used to remove batch effects with the
924 scanpy.external.pp.bbknn function with default parameters.

925 Visualization and clustering

926 UMAP[94] provided by scanpy was used to visualize data with default
927 parameters. K-nearest neighbor and Leiden clustering were applied
928 sequentially to cluster cells into groups. K-nearest neighbor graph
929 construction was done by scanpy.pp.neighbors with parameters
930 n_neighbors=12 and n_pcs=70. Leiden clustering was then performed by
931 scanpy.tl.leiden with parameter resolution=0.15. To improve UMAP
932 visualization, scanpy.tl.paga was applied, and we trimmed unnecessary graph
933 edges by scanpy.tl.paga with threshold=0.018.

934 Marker genes and statistics

935 Wilcoxon rank-sum tests were applied to examine differentially expressed
936 genes. Clusters were selected from the result of Leiden clustering.
937 Differentially expressed genes of a cluster against other clusters were
938 identified by scanpy.tl.rank_genes_groups and scanpy.pl.rank_genes_groups.
939 P-values were collected for each cluster and transformed by negative $\log_{10}$ for
940 better visualization. The top 50 differentially expressed genes were visualized
941 in the figure.

942

943 **Immunofluorescent staining**

944 Dissected thymus lobes from C57BL/6 mice were cleaned of connective
945 tissue and fixed in 4% paraformaldehyde (Sigma) for 1 h at 4˚C, washed in
946 PBS, submerged in 10% sucrose, and then in 30% sucrose for 12 h each.
947 The tissue was then frozen in Tissue-Tek OCT compound (Sakura Fintek) for
948 cryostat sectioning. 10 or 20 μm thick sections were prepared with CryoStar
949 NX50 (ThermoFisher) on Superfrost PLUS (ThermoScientific) microscope

950 slides, dried overnight, and stored at -80˚C until used. Before staining, the
951 sections were fixed with acetone (Sigma) at -20˚C for 10 min, air-dried, then
952 blocked with 5% goat serum + 5% donkey serum (both from Jackson
953 Immunoresearch) in PBS for 2 h and stained with primary antibodies: rat
954 monoclonal to MerTK (DS5MMER, eBioscience), rat monoclonal to TIM4
955 (RMT4-54, Bio-X-Cell) or rabbit polyclonal to Keratin 5 (BioLegend) overnight
956 at 4˚C in a humidified chamber. After washing in PBS, the sections were
957 labeled with goat anti-rat-Alexa Fluor 647 (Invitrogen) or goat anti-rat Cy3
958 (Jackson Immunoresearch) and donkey anti-rabbit AF647 (Jackson
959 Immunoresearch) secondary antibodies for 2 hours at room temperature,
960 followed by 5 min staining with DAPI. TUNEL Assay was done with the Click-
961 iT Plus TUNEL Assay Alexa Fluor 647 kit (Invitrogen) according to the
962 manufacturer's recommendations. A positive (pre-incubation with DNase I for
963 30 min at room temperature) and negative (no TdT enzyme) controls were
964 always included. The sections were mounted with 0.1% n-propyl gallate
965 (Sigma) in glycerol (Sigma) and imaged with an AxioObserver 7 (Carl Zeiss)
966 wide-field microscope equipped with Plan Apochromat 20x NA=0.8 objective
967 (Zeiss) and AxioCam 702 mono camera (Zeiss) and controlled by Zen 2.3
968 Blue (Zeiss) software. Image analysis was performed with Imaris 8.0.2
969 (Bitplane).
970
971 The co-localization scoring for MerTK and TIM4 with TUNEL was done with
972 Imaris 8.2 (Bitplane). TUNEL$^+$ cells were detected with the Spots function,
973 while MerTK$^+$ and TIM4$^+$ cells were detected with the Surface function. Spots
974 that co-localize with Surfaces were identified with the "Find Spots close to

975 Surface” function of Imaris XT. The threshold for co-localization was set to 5
976 µm. The results were manually curated so that Spots categorized as “not co-
977 localized” that were: 1) at the edge of the imaging field were excluded from
978 consideration; 2) with clear Surface signal around them were re-categorized
979 as "co-localized". The ratio of co-localized Spots to all Spots was calculated
980 and presented as the co-localization index.
981
982 **Thymus transplantation**
983 To obtain E15.5 embryos, *ROSA26*^{GFP} homozygous male and C57BL/6
984 female mice were mated in a cage overnight and separated on the next day.
985 Pregnant mice were sacrificed 15 days later, the viable embryos were
986 harvested, and the thymuses were isolated in ice-cold PBS. C57BL/6
987 recipients were anesthetized by i.p injection of Ketamine hydrochloride (120
988 µg/g, Toronto Research Chemicals) and Xylazine hydrochloride (12 µg/g,
989 Sigma). The fur on the left flank was removed, and the left kidney was
990 exposed by cutting the skin, muscle layer, and peritoneum. The kidney
991 capsule was nicked with a G23 needle, and the fetal thymus was pushed into
992 the pocket under the kidney capsule with a G23 needle equipped with a
993 plunger from a spinal needle. After the kidney was re-positioned back into the
994 peritoneal cavity, the peritoneum was sutured, and the skin was stapled with
995 metal clips. Rymadil (Carprofen, 5 µg/g, Zoetis) was given subcutaneously to
996 ease the wound pain, and Trimerin (Sulfadiazine at 0.5 mg/mL + Trimethoprim
997 at 0.1 mg/mL) were given in the drinking water for the first two weeks after the
998 surgery. The metal clips were removed from the skin after the first week, and

999 the transplanted thymus and recipient's endogenous thymus were harvested
1000 and analyzed six weeks after the kidney transplantation.
1001
1002 **Statistical analysis**
1003 Comparison between groups was made with Prism 6 (GraphPad Software).
1004 Comparisons between two groups were carried out with unpaired Student's t-
1005 test. When more than two groups were compared, a one-way ANOVA with
1006 Tukey correction was used. Differences were considered significant if $p<0.05$.
1007
1008 **Data availability**
1009 The RNA Sequencing data of thymic macrophages and thymic dendritic
1010 cells is available at NCBI Gene Expression Omnibus (GEO) as part of
1011 GSE122108 and at www.immgen.org. The single cell RNA sequencing data is
1012 deposited at NCBI GEO under accession number GSE185460. The source
1013 data underlying Fig. 1g-h, Fig. 3c, f, i, Fig. 4b. f, h, Fig. 6b, d, Fig. 7b, d, e, Fig.
1014 S1h, Fig. S3c, and Fig. S4b, d, e, g are provided in the Source Data files. All
1015 other data supporting the findings of this study are available within the article
1016 and its figures and tables.
1017
1018 **Abbreviations:**
1019 cDC – classical dendritic cell
1020 DC – dendritic cell
1021 EdU – 5-Ethynyl-2'-deoxyuridine
1022 GO – gene ontology
1023 HSC – hematopoietic stem cell

1024 IFN-I – type I Interferon

1025 IMMGEN – Immunological Genome Consortium

1026 scRNA-Seq – single-cell RNA sequencing

1027 TF – transcription factor

1028 ThyMacs – thymic macrophages

1029 TRA – tissue-restricted antigen

1030 YS – yolk sac

1031 **References:**

1032 1. Wynn TA, Chawla A, Pollard JW. Macrophage biology in development,
1033 homeostasis and disease. Nature. Nature Publishing Group; 2013;496:
1034 445–455. doi:10.1038/nature12034

1035 2. Baratin M, Simon L, Jorquera A, Ghigo C, Dembele D, Nowak J, et al. T
1036 Cell Zone Resident Macrophages Silently Dispose of Apoptotic Cells in
1037 the Lymph Node. Immunity. Elsevier Inc; 2017;47: 349–362.e5.
1038 doi:10.1016/j.immuni.2017.07.019

1039 3. A-Gonzalez N, Castrillo A. Origin and Specialization of Splenic
1040 Macrophages. Cellular Immunology. 2018;330: 1–27.
1041 doi:10.1016/j.cellimm.2018.05.005

1042 4. Bellomo A, Mondor I, Spinelli L, Lagueyrie M, Stewart BJ, Brouilly N, et
1043 al. Reticular Fibroblasts Expressing the Transcription Factor WT1
1044 Define a Stromal Niche that Maintains and Replenishes Splenic Red
1045 Pulp Macrophages. Immunity. Elsevier Inc; 2020;53: 127–142.e7.
1046 doi:10.1016/j.immuni.2020.06.008

1047 5. van Furth R, Cohn ZA. The origin and kinetics of mononuclear
1048 phagocytes. J Exp Med. Rockefeller University Press; 1968;128: 415–
1049 435. doi:10.1084/jem.128.3.415

1050 6. Ginhoux F, Guilliams M. Tissue-Resident Macrophage Ontogeny and
1051 Homeostasis. Immunity. 2016;44: 439–449.
1052 doi:10.1016/j.immuni.2016.02.024

1053 7. Perdiguero EG, Klapproth K, Schulz C, Busch K, Azzoni E, Crozet L, et
1054 al. Tissue-resident macrophages originate from yolk-sac-derived
1055 erythro-myeloid progenitors. Nat Immunol. Nature Publishing Group;
1056 2015;518: 547–551. doi:10.1038/nature13989

1057 8. Mass E, Ballesteros I, Farlik M, Halbritter F, Günther P, Crozet L, et al.

1058 Specification of tissue-resident macrophages during organogenesis.
1059 Science. American Association for the Advancement of Science;
1060 2016;353: aaf4238–aaf4238. doi:10.1126/science.aaf4238

1061 9. Ginhoux F, Greter M, Leboeuf M, Nandi S, See P, Gokhan S, et al. Fate
1062 mapping analysis reveals that adult microglia derive from primitive
1063 macrophages. Science. 2010;330: 841–845.
1064 doi:10.1126/science.1194637

1065 10. Hoeffel G, Wang Y, Greter M, See P, Teo P, Malleret B, et al. Adult
1066 Langerhans cells derive predominantly from embryonic fetal liver
1067 monocytes with a minor contribution of yolk sac–derived macrophages.
1068 J Exp Med. 2012;209: 1167–1181. doi:10.1084/jem.20120340

1069 11. Hoeffel G, Chen J, Lavin Y, Low D, Almeida FF, See P, et al. C-Myb(+)
1070 erythro-myeloid progenitor-derived fetal monocytes give rise to adult
1071 tissue-resident macrophages. Immunity. 2015;42: 665–678.
1072 doi:10.1016/j.immuni.2015.03.011

1073 12. Goldmann T, Wieghofer P, Jordão MJC, Prutek F, Hagemeyer N,
1074 Frenzel K, et al. Origin, fate and dynamics of macrophages at central
1075 nervous system interfaces. Nat Immunol. 2016;17: 797–805.
1076 doi:10.1038/ni.3423

1077 13. Hashimoto D, Chow A, Noizat C, Teo P, Beasley MB, Leboeuf M, et al.
1078 Tissue-Resident Macrophages Self-Maintain Locally throughout Adult
1079 Life with Minimal Contribution from Circulating Monocytes. Immunity.
1080 Elsevier Inc; 2013;38: 792–804. doi:10.1016/j.immuni.2013.04.004

1081 14. Epelman S, Lavine KJ, Beaudin AE, Sojka DK, Carrero JA, Calderon B,
1082 et al. Embryonic and Adult-Derived Resident Cardiac Macrophages Are
1083 Maintained through Distinct Mechanisms at Steady State and during
1084 Inflammation. Immunity. Elsevier Inc; 2014;40: 91–104.
1085 doi:10.1016/j.immuni.2013.11.019

1086 15. Sheng J, Ruedl C, Karjalainen K. Most Tissue-Resident Macrophages
1087 Except Microglia Are Derived from Fetal Hematopoietic Stem Cells.
1088 Immunity. Elsevier Inc; 2015;43: 382–393.
1089 doi:10.1016/j.immuni.2015.07.016

1090 16. Liu Z, Gu Y, Chakarov S, Bleriot C, Kwok I, Chen X, et al. Fate Mapping
1091 via Ms4a3-Expression History Traces Monocyte-Derived Cells. Cell.
1092 Elsevier; 2019;178: 1509–1525.e19. doi:10.1016/j.cell.2019.08.009

1093 17. Ensan S, Li A, Besla R, Degousee N, Cosme J, Roufaiel M, et al. Self-
1094 renewing resident arterial macrophages arise from embryonic
1095 CX3CR1+ precursors and circulating monocytes immediately after birth.
1096 Nat Immunol. Nature Publishing Group; 2015;17: 159–168.
1097 doi:10.1038/ni.3343

1098 18. Mondor I, Baratin M, Lagueyrie M, Saro L, Henri S, Gentek R, et al.

1099 Lymphatic Endothelial Cells Are Essential Components of the
1100 Subcapsular Sinus Macrophage Niche. Immunity. Elsevier Inc; 2019;50:
1101 1453–1466.e4. doi:10.1016/j.immuni.2019.04.002

1102 19. Molawi K, Wolf Y, Kandalla PK, Favret J, Hagemeyer N, Frenzel K, et
1103 al. Progressive replacement of embryo-derived cardiac macrophages
1104 with age. J Exp Med. 2014;211: 2151–2158. doi:10.1084/jem.20140639

1105 20. Heidt T, Courties G, Dutta P, Sager HB, Sebas M, Iwamoto Y, et al.
1106 Differential Contribution of Monocytes to Heart Macrophages in Steady-
1107 State and After Myocardial Infarction. Circulation Research. 2014;115:
1108 284–295. doi:10.1161/CIRCRESAHA.115.303567

1109 21. Yahara Y, Barrientos T, Tang YJ, Puviindran V, Nadesan P, Zhang H,
1110 et al. Erythromyeloid progenitors give rise to a population of osteoclasts
1111 that contribute to bone homeostasis and repair. Nat Cell Biol. Springer
1112 US; 2020;22: 1–28. doi:10.1038/s41556-019-0437-8

1113 22. Jacome-Galarza CE, Percin GI, Muller JT, Mass E, Lazarov T, Eitler J,
1114 et al. Developmental origin, functional maintenance and genetic rescue
1115 of osteoclasts. Nature. Nature Publishing Group; 2019;568: 541–545.
1116 doi:10.1038/s41586-019-1105-7

1117 23. Calderon B, Carrero JA, Ferris ST, Sojka DK, Moore L, Epelman S, et
1118 al. The pancreas anatomy conditions the origin and properties of
1119 resident macrophages. J Exp Med. 2015;212: 1497–1512.
1120 doi:10.1084/jem.20150496

1121 24. Tamoutounour S, Guilliams M, Sanchis FM, Liu H, Terhorst D, Malosse
1122 C, et al. Origins and Functional Specialization of Macrophages and of
1123 Conventional and Monocyte-Derived Dendritic Cells in Mouse Skin.
1124 Immunity. Elsevier Inc; 2013;39: 925–938.
1125 doi:10.1016/j.immuni.2013.10.004

1126 25. Bain CC, Bravo-Blas A, Scott CL, Gomez Perdiguero E, Geissmann F,
1127 Henri S, et al. Constant replenishment from circulating monocytes
1128 maintains the macrophage pool in the intestine of adult mice. Nat
1129 Immunol. 2014;15: 929–937. doi:10.1038/ni.2967

1130 26. Sierro F, Evrard M, Rizzetto S, Melino M, Mitchell AJ, Florido M, et al. A
1131 Liver Capsular Network of Monocyte-Derived Macrophages Restricts
1132 Hepatic Dissemination of Intraperitoneal Bacteria by Neutrophil
1133 Recruitment. Immunity. Elsevier Inc; 2017;47: 374–388.e6.
1134 doi:10.1016/j.immuni.2017.07.018

1135 27. Mossadegh-Keller N, Gentek R, Gimenez G, Bigot S, Mailfert S,
1136 Sieweke MH. Developmental origin and maintenance of distinct
1137 testicular macrophage populations. J Exp Med. 2017;214: 2829–2841.
1138 doi:10.1084/jem.20170829

1139 28. Lokka E, Lintukorpi L, Cisneros-Montalvo S, Mäkelä J-A, Tyystjärvi S,

1140 Ojasalo V, et al. Generation, localization and functions of macrophages
1141 during the development of testis. Nature Communications. Springer US;
1142 2020;11: 1–16. doi:10.1038/s41467-020-18206-0

1143 29. Wang M, Yang Y, Cansever D, Wang Y, Kantores C, Messiaen S, et al.
1144 Two populations of self-maintaining monocyte-independent
1145 macrophages exist in adult epididymis and testis. PNAS. 2020;118:
1146 e2013686117. doi:10.1073/pnas.2013686117/-/DCSupplemental

1147 30. Bain CC, Hawley CA, Garner H, Scott CL, Schridde A, Steers NJ, et al.
1148 Long-lived self-renewing bone marrow-derived macrophages displace
1149 embryo-derived cells to inhabit adult serous cavities. Nature
1150 Communications. Nature Publishing Group; 2016;7: 1–14.
1151 doi:10.1038/ncomms11852

1152 31. Surh CD, Sprent J. T-cell apoptosis detected in situ during positive and
1153 negative selection in the thymus. Nature. 1994;372: 100–103.
1154 doi:10.1038/372100a0

1155 32. Esashi E, Sekiguchi T, Ito H, Koyasu S, Miyajima A. Cutting Edge: A
1156 possible role for CD4+ thymic macrophages as professional scavengers
1157 of apoptotic thymocytes. Journal of Immunology (Baltimore, Md : 1950).
1158 American Association of Immunologists; 2003;171: 2773–2777.
1159 doi:10.4049/jimmunol.171.6.2773

1160 33. Liu L-T, Lang Z-F, Li Y, Zhu Y-J, Zhang J-T, Guo S-F, et al.
1161 Composition and characteristics of distinct macrophage subpopulations
1162 in the mouse thymus. Molecular Medicine Reports. 2013;7: 1850–1854.
1163 doi:10.3892/mmr.2013.1448

1164 34. Guerri L, Peguillet I, Geraldo Y, Nabti S, Premel V, Lantz O. Analysis of
1165 APC types involved in CD4 tolerance and regulatory T cell generation
1166 using reaggregated thymic organ cultures. J Immunol. American
1167 Association of Immunologists; 2013;190: 2102–2110.
1168 doi:10.4049/jimmunol.1202883

1169 35. Lopes N, Charaix J, Cédile O, Sergé A, Irla M. Lymphotoxin alpha fine-
1170 tunes T cell clonal deletion by regulating thymic entry of antigen-
1171 presenting cells. Nature Communications. Springer US; 2018;9: 1–16.
1172 doi:10.1038/s41467-018-03619-9

1173 36. Kim H-J, Alonzo ES, Dorothee G, Pollard JW, Sant'Angelo DB.
1174 Selective depletion of eosinophils or neutrophils in mice impacts the
1175 efficiency of apoptotic cell clearance in the thymus. Kim H-J, Alonzo ES,
1176 Dorothee G, Pollard JW, Sant'Angelo DB, editors. PLoS ONE. 2010;5:
1177 e11439. doi:10.1371/journal.pone.0011439.g010

1178 37. Tacke R, Hilgendorf I, Garner H, Waterborg C, Park K, Nowyhed H, et
1179 al. The transcription factor NR4A1 is essential for the development of a
1180 novel macrophage subset in the thymus. Sci Rep. 2015;5: 10055.
1181 doi:10.1038/srep10055

1182 38. Gautier EL, Shay T, Miller J, Greter M, Jakubzick C, Ivanov S, et al.
1183 Gene-expression profiles and transcriptional regulatory pathways that
1184 underlie the identity and diversity of mouse tissue macrophages. Nat
1185 Immunol. 2012;13: 1118–1128. doi:10.1038/ni.2419

1186 39. Ingersoll MA, Spanbroek R, Lottaz C, Gautier EL, Frankenberger M,
1187 Hoffmann R, et al. Comparison of gene expression profiles between
1188 human and mouse monocyte subsets. Blood. 2010;115: e10–e19.
1189 doi:10.1182/blood-2009-07-235028

1190 40. Wang H, Breed ER, Lee YJ, Qian LJ, Jameson SC, Hogquist KA.
1191 Myeloid cells activate iNKT cells to produce IL-4 in the thymic medulla.
1192 Proc Natl Acad Sci. National Academy of Sciences; 2019;116: 22262–
1193 22268. doi:10.1073/pnas.1910412116

1194 41. Chan CT, Fenn AM, Harder NK, Mindur JE, McAlpine CS, Patel J, et al.
1195 Liver X receptors are required for thymic resilience and T cell output. J
1196 Exp Med. 2020;217: 245–23. doi:10.1084/jem.20200318

1197 42. Wada H, Masuda K, Satoh R, Kakugawa K, Ikawa T, Katsura Y, et al.
1198 Adult T-cell progenitors retain myeloid potential. Nature. Nature
1199 Publishing Group; 2008;452: 768–772. doi:10.1038/nature06839

1200 43. Bell JJ, Bhandoola A. The earliest thymic progenitors for T cells
1201 possess myeloid lineage potential. Nature. 2008;452: 764–767.
1202 doi:10.1038/nature06840

1203 44. Schlenner SM, Madan V, Busch K, Tietz A, LAufle C, Costa C, et al.
1204 Fate Mapping Reveals Separate Origins of T Cells and Myeloid
1205 Lineages in the Thymus. Immunity. Elsevier Ltd; 2010;32: 426–436.
1206 doi:10.1016/j.immuni.2010.03.005

1207 45. Witmer-Pack MD, Hughes DA, Schuler G, Lawson L, McWilliam A,
1208 Inaba K, et al. Identification of macrophages and dendritic cells in the
1209 osteopetrotic (op/op) mouse. J Cell Sci. 1993;104 (Pt 4): 1021–1029.

1210 46. Sasmono RT, Oceandy D, Pollard JW, Tong W, Pavli P, Wainwright BJ,
1211 et al. A macrophage colony-stimulating factor receptor-green
1212 fluorescent protein transgene is expressed throughout the mononuclear
1213 phagocyte system of the mouse. Blood. American Society of
1214 Hematology; 2003;101: 1155–1163. doi:10.1182/blood-2002-02-0569

1215 47. Hume DA. Applications of myeloid-specific promoters in transgenic mice
1216 support in vivo imaging and functional genomics but do not support the
1217 concept of distinct macrophage and dendritic cell lineages or roles in
1218 immunity. Journal of Leukocyte Biology. 2011;89: 525–538.
1219 doi:10.1189/jlb.0810472

1220 48. Taniuchi I, Osato M, Egawa T, Sunshine MJ, Bae SC, Komori T, et al.
1221 Differential requirements for Runx proteins in CD4 repression and
1222 epigenetic silencing during T lymphocyte development. Cell. 2002;111:

621–633. doi:10.1016/s0092-8674(02)01111-x

49. Ebihara T, Song C, Ryu SH, Plougastel-Douglas B, Yang L, Levanon D, et al. Runx3 specifies lineage commitment of innate lymphoid cells. Nat Immunol. Nature Publishing Group; 2015;16: 1124–1133. doi:10.1038/ni.3272

50. Fainaru O, Woolf E, Lotem J, Yarmus M, Brenner O, Goldenberg D, et al. Runx3 regulates mouse TGF-beta-mediated dendritic cell function and its absence results in airway inflammation. EMBO J. John Wiley & Sons, Ltd; 2004;23: 969–979. doi:10.1038/sj.emboj.7600085

51. Kohyama M, Ise W, Edelson BT, Wilker PR, Hildner K, Mejia C, et al. Role for Spi-C in the development of red pulp macrophages and splenic iron homeostasis. Nat Immunol. Nature Publishing Group; 2008;457: 318–321. doi:10.1038/nature07472

52. Haldar M, Kohyama M, So AY-L, KC W, Wu X, Briseño CG, et al. Heme-Mediated SPI-C Induction Promotes Monocyte Differentiation into Iron-Recycling Macrophages. Cell. Elsevier Inc; 2014;156: 1223–1234. doi:10.1016/j.cell.2014.01.069

53. Yona S, Kim K-W, Wolf Y, Mildner A, Varol D, Breker M, et al. Fate Mapping Reveals Origins and Dynamics of Monocytes and Tissue Macrophages under Homeostasis. Immunity. Elsevier; 2013;38: 79–91. doi:10.1016/j.immuni.2012.12.001

54. McCaughtry TM, Wilken MS, Hogquist KA. Thymic emigration revisited. J Exp Med. 2007;204: 2513–2520. doi:10.1084/jem.20070601

55. Lienenklaus S, Cornitescu M, Ziętara N, Łyszkiewicz M, Gekara N, Jabłónska J, et al. Novel reporter mouse reveals constitutive and inflammatory expression of IFN-beta in vivo. J Immunol. American Association of Immunologists; 2009;183: 3229–3236. doi:10.4049/jimmunol.0804277

56. Otero DC, Baker DP, David M. IRF7-dependent IFN-β production in response to RANKL promotes medullary thymic epithelial cell development. J Immunol. American Association of Immunologists; 2013;190: 3289–3298. doi:10.4049/jimmunol.1203086

57. Breed ER, Lee ST, Hogquist KA. Directing T cell fate: How thymic antigen presenting cells coordinate thymocyte selection. Seminars in Cell and Developmental Biology. Elsevier Ltd; 2017;: 1–9. doi:10.1016/j.semcdb.2017.07.045

58. Kurd NS, Lutes LK, Yoon J, Chan SW, Dzhagalov IL, Hoover AR, et al. A role for phagocytosis in inducing cell death during thymocyte negative selection. eLife. 2019;8: 1879–18. doi:10.7554/eLife.48097

59. Morioka S, Perry JSA, Raymond MH, Medina CB, Zhu Y, Zhao L, et al. Efferocytosis induces a novel SLC program to promote glucose uptake

and lactate release. Nature. Springer US; 2018;563: 1–21. doi:10.1038/s41586-018-0735-5

60. Bleriot C, Chakarov S, Ginhoux F. Determinants of Resident Tissue Macrophage Identity and Function. Immunity. Elsevier Inc; 2020;52: 957–970. doi:10.1016/j.immuni.2020.05.014

61. Stritesky GL, Xing Y, Erickson JR, Kalekar LA, Wang X, Mueller DL, et al. Murine thymic selection quantified using a unique method to capture deleted T cells. Proc Natl Acad Sci. 2013;110: 4679–4684. doi:10.1073/pnas.1217532110

62. Baba T, Nakamoto Y, Mukaida N. Crucial Contribution of Thymic Sirp + Conventional Dendritic Cells to Central Tolerance against Blood-Borne Antigens in a CCR2-Dependent Manner. J Immunol. 2009;183: 3053–3063. doi:10.4049/jimmunol.0900438

63. Gallegos AM, Bevan MJ. Central Tolerance to Tissue-specific Antigens Mediated by Direct and Indirect Antigen Presentation. J Exp Med. 2004;200: 1039–1049. doi:10.1084/jem.20041457

64. Koble C, Kyewski B. The thymic medulla: a unique microenvironment for intercellular self-antigen transfer. J Exp Med. 2009;206: 1505–1513. doi:10.1084/jem.20082449

65. Vobořil M, Brabec T, Dobeš J, Šplíchalová I, Březina J, Čepková A, et al. Toll-like receptor signaling in thymic epithelium controls monocyte-derived dendritic cell recruitment and Treg generation. Nature Communications. Springer US; 2020;11: 1–16. doi:10.1038/s41467-020-16081-3

66. Dixit VD. Impact of immune-metabolic interactions on age-related thymic demise and T cell senescence. Semin Immunol. Elsevier Ltd; 2012;24: 321–330. doi:10.1016/j.smim.2012.04.002

67. Rivera-Gonzalez GC, Shook BA, Andrae J, Holtrup B, Bollag K, Betsholtz C, et al. Skin Adipocyte Stem Cell Self-Renewal Is Regulated by a PDGFA/AKT-Signaling Axis. Stem Cell. Elsevier Inc; 2016;19: 738–751. doi:10.1016/j.stem.2016.09.002

68. Olson LE, Soriano P. Increased PDGFRα Activation Disrupts Connective Tissue Development and Drives Systemic Fibrosis. Developmental Cell. Elsevier Ltd; 2009;16: 303–313. doi:10.1016/j.devcel.2008.12.003

69. Satpathy AT, KC W, Albring JC, Edelson BT, Kretzer NM, Bhattacharya D, et al. Zbtb46expression distinguishes classical dendritic cells and their committed progenitors from other immune lineages. J Exp Med. 2012;209: 1135–1152. doi:10.1084/jem.20120030

70. Guilliams M, Mildner A, Yona S. Developmental and Functional Heterogeneity of Monocytes. Immunity. Elsevier Inc; 2018;49: 595–613.

1305 doi:10.1016/j.immuni.2018.10.005

1306 71. Tabula Muris Consortium. Single-cell transcriptomics of 20 mouse
1307 organs creates a Tabula Muris. Nature. Nature Publishing Group;
1308 2018;562: 367–372. doi:10.1038/s41586-018-0590-4

1309 72. Han X, Wang R, Zhou Y, Fei L, Sun H, Lai S, et al. Mapping the Mouse
1310 Cell Atlas by Microwell-Seq. Cell. Elsevier Inc; 2018;172: 1091–
1311 1097.e17. doi:10.1016/j.cell.2018.02.001

1312 73. Tabula Muris Consortium. A single-cell transcriptomic atlas
1313 characterizes ageing tissues in the mouse. Nature. Nature Publishing
1314 Group; 2020;583: 590–595. doi:10.1038/s41586-020-2496-1

1315 74. Kernfeld EM, Genga RMJ, Neherin K, Magaletta ME, Xu P, Maehr R. A
1316 Single-Cell Transcriptomic Atlas of Thymus Organogenesis Resolves
1317 Cell Types and Developmental Maturation. Immunity. Elsevier Inc;
1318 2018;: 1–33. doi:10.1016/j.immuni.2018.04.015

1319 75. Park J-E, Botting RA, Domínguez Conde C, Popescu D-M, Lavaert M,
1320 Kunz DJ, et al. A cell atlas of human thymic development defines T cell
1321 repertoire formation. Science. American Association for the
1322 Advancement of Science; 2020;367: eaay3224–12.
1323 doi:10.1126/science.aay3224

1324 76. Bornstein C, Nevo S, Giladi A, Kadouri N, Pouzolles M, Gerbe F, et al.
1325 Single-cell mapping of the thymic stroma identifies IL-25-producing tuft
1326 epithelial cells. Nature. Springer US; 2018;559: 1–25.
1327 doi:10.1038/s41586-018-0346-1

1328 77. Bautista JL, Cramer NT, Miller CN, Chavez J, Berrios DI, Byrnes LE, et
1329 al. Single-cell transcriptional profiling of human thymic stroma uncovers
1330 novel cellular heterogeneity in the thymic medulla. Nature
1331 Communications. Nature Publishing Group; 2021;12: 1096–15.
1332 doi:10.1038/s41467-021-21346-6

1333 78. Burnett SH, Kershen EJ, Zhang J, Zeng L, Straley SC, Kaplan AM, et
1334 al. Conditional macrophage ablation in transgenic mice expressing a
1335 Fas-based suicide gene. Journal of Leukocyte Biology. Society for
1336 Leukocyte Biology; 2004;75: 612–623. doi:10.1189/jlb.0903442

1337 79. Jung S, Aliberti J, Graemmel P, Sunshine MJ, Kreutzberg GW, Sher A,
1338 et al. Analysis of fractalkine receptor CX(3)CR1 function by targeted
1339 deletion and green fluorescent protein reporter gene insertion. Mol Cell
1340 Biol. 2000;20: 4106–4114.

1341 80. Lindquist RL, Shakhar G, Dudziak D, Wardemann H, Eisenreich T,
1342 Dustin ML, et al. Visualizing dendritic cell networks in vivo. Nat
1343 Immunol. 2004;5: 1243–1250. doi:10.1038/ni1139

1344 81. Faust N, Varas F, Kelly LM, Heck S, Graf T. Insertion of enhanced
1345 green fluorescent protein into the lysozyme gene creates mice with

1346 green fluorescent granulocytes and macrophages. Blood. 2000;96:
1347 719–726.

1348 82. Roesch K, Jadhav AP, Trimarchi JM, Stadler MB, Roska B, Sun BB, et
1349 al. The transcriptome of retinal Müller glial cells. J Comp Neurol.
1350 2008;509: 225–238. doi:10.1002/cne.21730

1351 83. Madisen L, Zwingman TA, Sunkin SM, Oh SW, Zariwala HA, Gu H, et
1352 al. A robust and high-throughput Cre reporting and characterization
1353 system for the whole mouse brain. Nature Neuroscience. Nature
1354 Publishing Group; 2009;13: 133–140. doi:10.1038/nn.2467

1355 84. Picelli S, Faridani OR, rklund ASKBO, Winberg GOS, Sagasser S,
1356 Sandberg R. Full-length RNA-seq from single cells using Smart-seq2.
1357 Nature Protocols. Nature Publishing Group; 2014;9: 171–181.
1358 doi:10.1038/nprot.2014.006

1359 85. Picelli S, Björklund ÅK, Faridani OR, Sagasser S, Winberg G, Sandberg
1360 R. Smart-seq2 for sensitive full-length transcriptome profiling in single
1361 cells. Nat Meth. 2013;10: 1096–1098. doi:10.1038/nmeth.2639

1362 86. Love MI, Huber W, Anders S. Moderated estimation of fold change and
1363 dispersion for RNA-seq data with DESeq2. Genome Biol. BioMed
1364 Central; 2014;15: 31–21. doi:10.1186/s13059-014-0550-8

1365 87. Schmeier S, Alam T, Essack M, Bajic VB. TcoF-DB v2: update of the
1366 database of human and mouse transcription co-factors and transcription
1367 factor interactions. Nucleic Acids Res. 2017;45: D145–D150.
1368 doi:10.1093/nar/gkw1007

1369 88. Reich M, Liefeld T, Gould J, Lerner J, Tamayo P, Mesirov JP.
1370 GenePattern 2.0. Nat Genet. Nature Publishing Group; 2006;38: 500–
1371 501. doi:10.1038/ng0506-500

1372 89. Yu G, Wang L-G, Han Y, He Q-Y. clusterProfiler: an R Package for
1373 Comparing Biological Themes Among Gene Clusters. OMICS: A
1374 Journal of Integrative Biology. Mary Ann Liebert, Inc., publishers;
1375 2012;16: 284–287. doi:10.1089/omi.2011.0118

1376 90. Heyne GW, Plisch EH, Melberg CG, Sandgren EP, Peter JA, Lipinski
1377 RJ. A Simple and Reliable Method for Early Pregnancy Detection in
1378 Inbred Mice. J Am Assoc Lab Anim Sci. 2015;54: 368–371.

1379 91. Iturri L, Saenz Coronilla J, Lallemand Y, Gomez Perdiguero E.
1380 Identification Of Erythromyeloid Progenitors And Their Progeny In The
1381 Mouse Embryo By Flow Cytometry. JoVE. 2017;: 1–10.
1382 doi:10.3791/55305

1383 92. Wolf FA, Angerer P, Theis FJ. SCANPY: large-scale single-cell gene
1384 expression data analysis. Genome Biol. BioMed Central; 2018;19: 15–
1385 5. doi:10.1186/s13059-017-1382-0

93. Polański K, Young MD, Miao Z, Meyer KB, Teichmann SA, Park J-E. BBKNN: fast batch alignment of single cell transcriptomes. Bioinformatics. 2019;36: 964–965. doi:10.1093/bioinformatics/btz625#supplementary-data

94. McInnes L, Healy J, Melville J. UMAP: Uniform Manifold Approximation and Projection for Dimension Reduction. ArXiv e-prints. 2018. doi:1802.03426v3

Acknowledgments

We are grateful to the IMMGEN consortium for performing the RNA sequencing of our samples and providing access to its database. We thank the following core facilities at National Yang-Ming Chiao-Tung University: Instrumentation Resource Center for providing access to its sorting and imaging facility and the Animal Facility for mouse husbandry. We are very grateful to Wan-Chun Chang, Bing-Xiu Guo, Chien-Yi Tung, and Kate Hua from the Genomics Center for Clinical and Biotechnological Applications of NCFB (NYCU, Taipei) for help with scRNA-Seq. Special thanks go to Dr. Fang Liao, Academia Sinica, Taipei, for help with cell sorting and for providing the 24G2 hybridoma, and Chang-Feng Chu for technical assistance. We are very grateful to Ms. Su-Hua Jiang at Veterans General Hospital, Taipei, for help with using the irradiator. Some figures were made with BioRender.

This work was supported by the Ministry of Science and Technology (grants # 106-2320-B-010 -026 -MY3, and 107-2320-B-010 -016 -MY3 to IL Dzhagalov and grants # 107-2320-B-010-020, and 108-2628-B-010-005 to CL Hsu), the Yen-Tjing Ling Medical Foundation (grants # CI-107-6 and CI-108-5 to IL Dzhagalov), and the Cancer Progression Research Center (NYCU). The authors declare no competing financial interests.

Author contributions

TA Zhou designed experiments, performed research, analyzed and interpreted data, and wrote the manuscript; HP Hsu and CY Lin performed research, analyzed and interpreted data; YH Tu and HC Huang analyzed the scRNA-Seq data; NJ Chen, JW Tsai, EA Robey, and CL Hsu provided expertise, shared critical reagents, and edited the manuscript; IL Dzhagalov conceptualized the studies, designed experiments, performed research, analyzed, interpreted the data, and wrote the manuscript.

Supplementary figures and tables

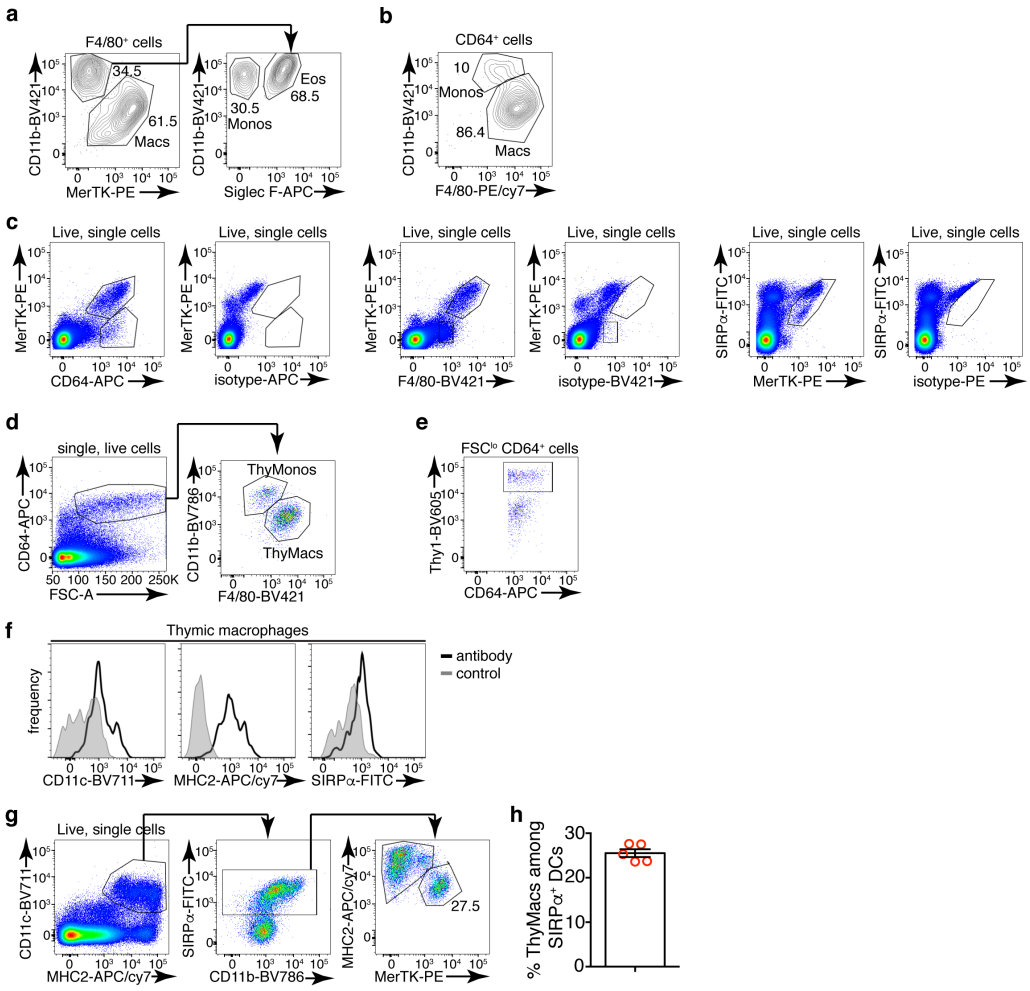

1424 **Figure 1 – Figure supplement 1: Phenotype of thymic macrophages**
1425 **and other myeloid cells positive for F4/80 and CD64. a** Example flow
1426 cytometry plots breaking down F4/80^{+} cells in the thymus into macrophages
1427 (MerTK^{+}), eosinophils (CD11b^{+}MerTK^{-}Siglec F^{+}) and monocytes
1428 (CD11b^{+}MerTK^{-}Siglec F^{-}). **b** An example flow cytometry plot dividing CD64+
1429 cells into macrophages (F4/80^{+}CD11b^{lo}) and monocytes (CD11b^{+}F4/80^{lo}). **c**
1430 Representative flow cytometry staining of enzymatically digested thymus
1431 single-cell suspension for CD64, MerTK, and F4/80 and respective isotype
1432 controls. **d** Gating strategy routinely used to identify thymic macrophages as
1433 CD64^{+}F4/80^{+}CD11b^{lo}FSC^{hi} cells. **e** Example flow cytometry plots showing that
1434 CD64^{+}FSC^{lo} cells include Thy1^{+} cells (most likely thymocytes). **f** Expression of
1435 CD11c, MHC2, and SIRPα on ThyMacs with respective controls. **g** Example
1436 flow cytometry plots showing that gating on CD11c^{+}MHC2^{+} thymus cells, in
1437 addition to DCs, also includes macrophages, especially among SIRPα^{+} cells.
1438 **h** Frequency of MerTK^{+} cells among CD11c^{+}MHC2^{+}SIRPα^{+} cells. The data
1439 are mean±SEM from 5 individual mice. Each dot is an individual mouse. The
1440 flow cytometry plots are representative of ≥5 individual experiments.

1441

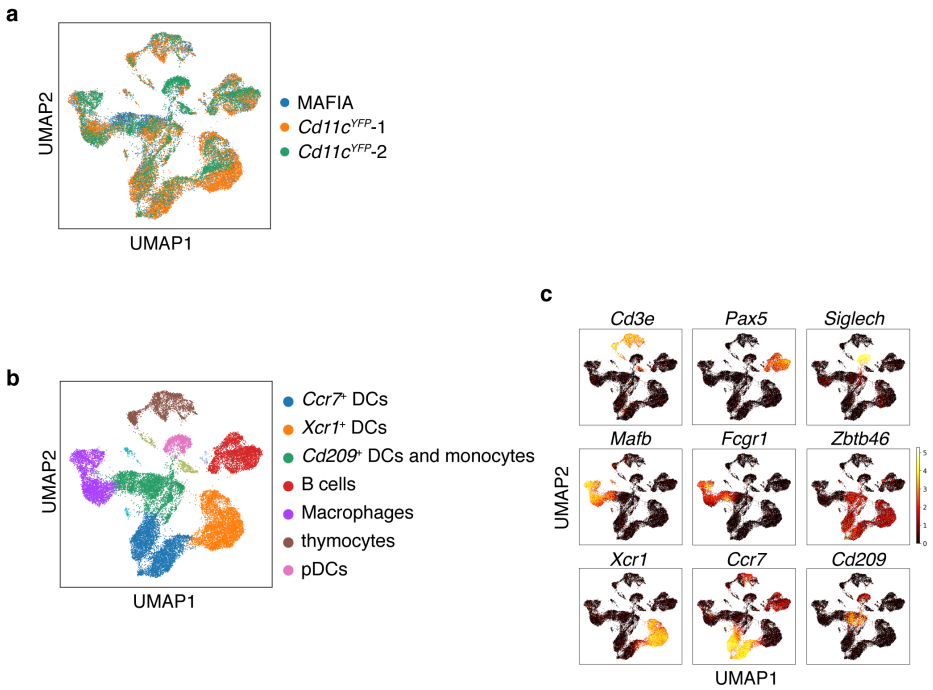

1442 **Figure 1 – Figure Supplement 2: UMAP clustering of single-cell RNA-**

1443 **Sequencing (scRNA-Seq) data. a** Clustering of the scRNA-Seq data shows

1444 that the cells from the three samples (one from GFP$^+$ cells in MAFIA mice and

1445 two from YFP$^+$ cells in *Cd11c^{YFP}* mice) overlap considerably. **b** Identification of

1446 the clusters from the scRNA-Seq data based on lineage-specific markers. **c**

1447 Expression of lineage-specific markers in different clusters.

1448

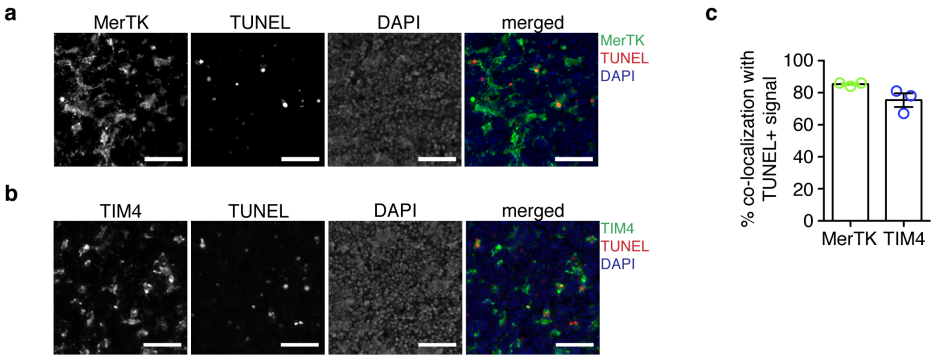

1449 **Figure 1 – Figure Supplement 3: Most TUNEL⁺ apoptotic cells co-**

1450 **localize with thymic macrophages. a** Example images showing co-

1451 localization of TUNEL⁺ apoptotic cells and MerTK⁺ ThyMacs. **b** Example

1452 images showing co-localization of TUNEL⁺ apoptotic cells and TIM4⁺

1453 ThyMacs. Scale bars in **a** and **b** are 50 μm. **c** Frequencies of the co-

1454 localization of TUNEL⁺ signal with MerTK⁺ and TIM4⁺ cells. All

1455 immunofluorescent images are representative of at least 3 independent

1456 repeats. Data in **c** represent mean±SEM. Each dot is an individual mouse.

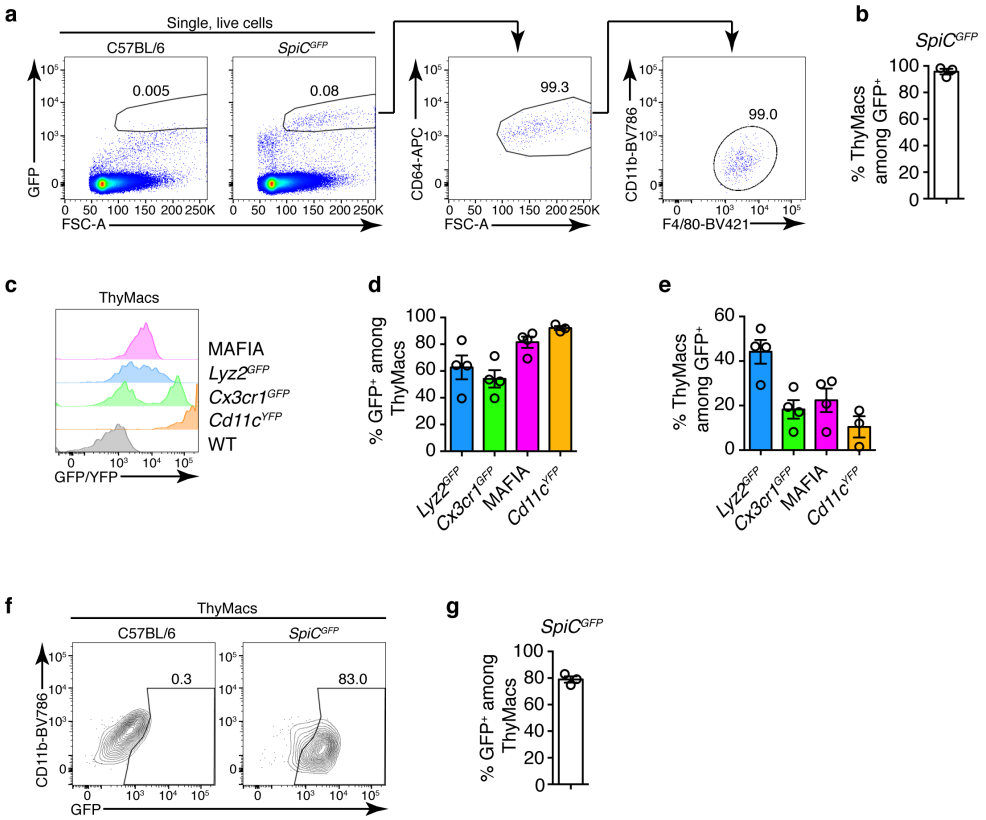

1457 **Figure 2 – Figure Supplement 1: Expression of *Spic*^{GFP} marks most**
1458 **thymic macrophages. a** Example of the gating strategy to identify ThyMacs
1459 among *Spic*$^{GFP+}$ cells. **b** Frequencies of ThyMacs among *Spic*$^{GFP+}$ cells. **c**
1460 Representative flow cytometry plots of the expression of four reporter alleles
1461 in ThyMacs. **d** Frequencies of GFP/YFP^{+} cells among ThyMacs. **e**
1462 Frequencies of ThyMacs among GFP/YFP^{+} cells. **f** Representative flow
1463 cytometry plots of the expression of *Spic*^{GFP} in ThyMacs. **g** Frequencies of
1464 *Spic*$^{GFP+}$ cells among ThyMacs. All flow cytometry plots are representative of
1465 at least 3 independent repeats. Data in **b**, **d**, **e**, and **f** represent mean±SEM.
1466 Each dot is an individual mouse. The numbers in the flow cytometry plots are
1467 the percent of cells in the respective gate.
1468

Table S1: E**xpression of differentially up-regulated transcription factors in thymic macrophages**

Gene name	ThyMacs	non-ThyMacs
Irf7	3879.32	300.82
Irf8	3528.27	1474.35
Stat1	2403.69	522.04
Dnmt3a	1515.94	647.81
Znxf1	1379.89	635.36
Stat2	1210.35	472.53
Nr1h3	1182.17	147.05
Srebf1	975.09	399.06
Rxra	760.26	298.55
Trps1	746.36	232.48
Runx3	723.14	9.76
Relb	715.53	293.92
Sp100	696.94	324.47
Zbp1	639.19	69.83
Tfec	588.72	74.66
Spic	573.11	34.36
Nfkbie	569.74	226.76
Ncoa4	550.69	249.15
Rest	548.22	269.22
Meis3	530.8	120.91
Bhlhe40	490.59	99.56
Parp12	414.11	126.82
Arid5b	374.03	177.08
Creb5	295.14	47.91
Pparg	276.54	33.24

1469 **Figure 2 – Table Supplement 1: Expression of differentially up-**
1470 **regulated transcription factors in thymic macrophages.** Transcription
1471 factors that were highly expressed in thymic macrophages (>250) and up-

1472 regulated >2-fold in thymic macrophages compared to non-thymic

1473 macrophages were listed alphabetically, and the geometric mean of 4

1474 replicates of thymic macrophages (ThyMacs) and two replicates of each of the

1475 9 non-thymic macrophage populations (non-ThyMacs) were recorded. Non-

1476 thymic macrophages are: spleen red pulp macrophages, Kupffer cells,

1477 bronchoalveolar lavage macrophages, peritoneal cavity macrophages, aorta

1478 macrophages, heart macrophages, white adipose tissue macrophages,

1479 central nervous system microglia, spinal cord macrophages.

Table S2. **List of the differentially expressed genes among *Timd*4+ thymic macrophages, *Cx3cr1*+ thymic macrophages, and thymic monocytes**

CX3CR1+ ThyMacs		**Tim4+ ThyMacs**		**ThyMonos**	
Gene name	adjusted p-value	Gene name	adjusted p-value	Gene name	adjusted p-value
Ctsz	0	*Hpgd*	0	*Alox5ap*	0
Cd63	0	*Serpinb6a*	0	*S100a6*	0
Pmepa1	0	*Slc40a1*	0	*Ly6c2*	0
Zmynd15	0	*Cd81*	0	*Ifi27l2a*	0
Olfml3	0	*Vcam1*	0	*Fau*	0
Mmp2	0	*Cfp*	0	*Coro1a*	0
AU020206	1.60E-290	*Spic*	0	*Ccr2*	0
Plxnd1	1.59E-285	*Trf*	0	*Rps27*	0
Cst7	8.68E-279	*Actn1*	0	*Tmsb10*	0
Dnase1l3	2.45E-270	*Maf*	0	*Ifitm2*	7.21E-302
Timp2	2.15E-267	*Pld3*	0	*Fxyd5*	6.36E-299
Lgals3bp	8.69E-263	*Il18*	0	*Rps19*	2.04E-292
Pdgfa	6.87E-255	*Mrc1*	0	*Rpl18*	6.50E-291
Mmp14	2.33E-253	*Crip2*	0	*Rpl9*	1.11E-289
Fam46c	9.99E-235	*Tmem65*	0	*Rps23*	1.28E-289
Chst2	1.19E-226	*Igf1*	0	*Napsa*	8.91E-279
Cp	5.36E-225	*Epb41l3*	0	*Ms4a4c*	8.25E-272
Camk1	7.12E-225	*Timd4*	0	*Plac8*	2.10E-270
B2m	1.09E-222	*Blvrb*	0	*Rpl18a*	9.26E-269
Lhfpl2	4.52E-217	*Clec1b*	0	*S100a4*	4.98E-268
Acp5	5.90E-216	*Cd68*	0	*Cd52*	3.67E-267
Lag3	3.91E-213	*Axl*	0	*Rps14*	1.94E-266
Lyz2	1.28E-209	*Paqr9*	3.32E-307	*Ifitm3*	3.19E-263
H2-M2	1.22E-199	*Sdc3*	3.45E-305	*Rpl34*	2.02E-261
Psap	7.26E-198	*Myo9a*	5.59E-305	*Rps27a*	3.67E-260
Gatm	1.33E-192	*Scp2*	3.79E-302	*Rpl36*	1.54E-259
Cpd	1.50E-192	*Selenop*	2.10E-295	*Rps16*	2.55E-258

C3	2.34E-187	*Lrp1*	2.08E-294	*Rpl24*	1.37E-257
Cxcl16	8.11E-183	*Lap3*	1.45E-290	*Rps9*	6.34E-253
Lgals3	1.57E-182	*Marcks*	2.77E-279	*Gpr141*	1.21E-246
Ube2j1	1.63E-180	*Glul*	3.64E-279	*Rpl27a*	3.06E-243
Plxnc1	9.84E-180	*Hebp1*	3.76E-278	*Rpl17*	8.15E-241
Stab1	4.07E-176	*Ear2*	4.53E-276	*Rps24*	1.46E-240
Cyth1	3.27E-163	*Apoc1*	2.49E-275	*Rps13*	2.34E-236
Spsb1	3.96E-163	*Kcna2*	3.72E-275	*Rpl38*	1.95E-226
Blnk	2.35E-162	*Myo10*	9.05E-269	*H2-DMb1*	1.02E-223
Cx3cr1	9.29E-162	*Atp13a2*	2.95E-267	*Rps18*	5.39E-223
Med10	5.25E-161	*Slc1a3*	6.24E-263	*Rpl19*	3.68E-221
Nek6	5.28E-160	*Slco2b1*	1.11E-258	*Rpl8*	2.01E-219
Ptms	1.05E-159	*mt-Nd2*	3.45E-258	*Rpl7a*	4.17E-217
Anxa5	1.10E-156	*Wwp1*	2.16E-253	*Gm34084*	5.23E-216
Gpnmb	1.21E-154	*Aplp2*	4.22E-248	*Rpl13*	2.08E-215
Itgb5	2.78E-154	*Atp8a1*	5.03E-248	*Rpl11*	2.47E-213
Myo5a	1.11E-146	*P2ry13*	3.17E-247	*Rpl35a*	2.13E-210
Runx3	1.81E-146	*Ccdc148*	4.70E-245	*Rpsa*	1.62E-209
Tmem176a	2.34E-144	*Grn*	1.58E-244	*Rpl6*	5.70E-208
Ctss	4.81E-141	*Bank1*	1.82E-239	*Tpt1*	2.63E-206
Sh3pxd2b	9.38E-141	*Mertk*	2.15E-238	*Rack1*	2.14E-203
Rtcb	4.42E-140	*Nr1h3*	1.13E-235	*Rpl23*	6.14E-199
Fam20c	1.91E-139	*Prnp*	2.93E-235	*Rpl26*	7.48E-198
Il2rg	8.84E-138	*Ninj1*	2.42E-234	*Rps6*	6.64E-197
Lpcat2	8.53E-137	*Fcna*	3.33E-233	*Rps10*	2.06E-195
Kynu	8.49E-136	*Csrp1*	1.16E-230	*Ier5*	1.06E-191
Tnfsf13b	8.77E-136	*Rgl1*	7.18E-229	*Rps3*	8.23E-185
Gpr157	1.18E-135	*Lpl*	4.94E-223	*Rpl27*	8.23E-185
Tgfbr1	7.63E-135	*Fam213b*	1.08E-222	*Rps5*	8.36E-185
H2-K1	1.15E-133	*Tcf7l2*	1.26E-222	*Rps7*	3.96E-182
Basp1	1.23E-133	*AB124611*	4.64E-221	*Rps15a*	6.82E-182
Pla2g7	1.80E-132	*Abcc3*	3.28E-216	*Rps11*	1.97E-180
Fth1	4.19E-131	*Fcgrt*	5.79E-216	*Rps4x*	5.07E-180
Ggh	1.85E-126	*Tgm2*	1.88E-215	*Rplp0*	3.09E-177
Adam19	6.94E-126	*Itgad*	5.35E-214	*Ly6i*	8.17E-176
C3ar1	7.35E-125	*Ptgs1*	2.94E-213	*S100a11*	6.23E-175
Ccl12	3.37E-123	*Laptm4a*	1.01E-212	*Atox1*	1.22E-174
Hvcn1	2.51E-121	*Comt*	1.33E-206	*Pim1*	9.56E-174
Anxa3	8.60E-121	*Creg1*	3.24E-205	*Sh3bgrl3*	3.97E-173
Tgfbi	1.88E-120	*Adgre1*	9.67E-205	*Ciita*	7.35E-173
Ctsd	2.73E-117	*Clec12a*	6.33E-204	*Eef1a1*	6.09E-172
Itm2c	5.19E-116	*Tspan4*	7.80E-203	*Rps3a1*	9.09E-168
Tmem119	5.62E-116	*Txn1*	9.13E-203	*Gm2a*	6.07E-165
Rap2a	1.03E-114	*Ctsb*	9.52E-201	*Ptprc*	2.05E-163
Ctsl	4.00E-114	*Mrap*	5.65E-197	*Rpl37*	1.51E-161
Itga6	1.83E-113	*Slc16a9*	5.99E-197	*Rps25*	3.03E-160

B4galnt1	2.45E-113	*Abcg3*	3.83E-196	*H3f3a*	5.92E-159
Fam3c	1.64E-112	*Pla2g15*	4.22E-196	*Btg2*	1.14E-158
Tmem173	1.54E-111	*C1qc*	6.17E-192	*Rpl15*	1.42E-158
Ski	3.59E-111	*Agpat3*	1.68E-191	*Cnn2*	1.09E-156
Anpep	5.85E-111	*Hs6st1*	1.95E-191	*Cdkn1a*	2.57E-156
Gng2	2.37E-110	*Dmpk*	2.15E-191	*Slfn1*	4.83E-155
Nceh1	2.88E-110	*Cd38*	1.79E-190	*Sem1*	4.08E-154
H2-Q7	4.94E-108	*Tmem26*	2.02E-189	*Lsp1*	1.34E-152
Rtn1	1.28E-106	*Slc11a1*	1.05E-188	*Rpl37a*	1.78E-152
Sorl1	1.31E-103	*Cd300a*	1.41E-187	*Rpl22*	3.64E-152
Glipr1	1.22E-102	*Slc7a7*	3.28E-187	*Sirpb1c*	4.81E-152
Gsn	2.00E-102	*Cyb5a*	6.94E-187	*Traf1*	6.97E-152
Afdn	4.54E-102	*Sipa1l1*	7.41E-187	*Emb*	4.22E-151
Ak2	1.11E-101	*Il18bp*	1.48E-186	*Rpl30*	1.32E-147
Ntpcr	2.21E-98	*Cd86*	2.52E-183	*Rps15*	1.14E-146
Scarb2	3.16E-97	*Vamp5*	3.05E-183	*H2-Ab1*	2.84E-145
Creb5	5.41E-97	*Jup*	6.69E-182	*Il1b*	3.05E-145
Gsto1	5.56E-97	*Blvra*	1.30E-178	*Rps28*	4.52E-145
Ncf1	4.26E-96	*Mgst1*	6.48E-178	*Jarid2*	1.82E-143
Ppfia4	4.97E-96	*Tbxas1*	1.47E-177	*Rps26*	1.53E-142
Chchd10	7.77E-96	*Hpgds*	2.04E-177	*Rpl32*	4.21E-142
Gna12	1.23E-95	*Tgfbr2*	2.70E-176	*Pld4*	9.07E-142
Mvb12b	1.80E-95	*Clec4n*	3.52E-175	*Cbfa2t3*	1.54E-141
Rasal3	1.45E-94	*Ms4a7*	5.30E-175	*Rps21*	4.04E-141
Scoc	6.86E-94	*Sirpa*	3.35E-171	*Fgr*	4.04E-141
Cfb	6.00E-93	*Fyn*	2.84E-168	*Rps8*	1.11E-139
Lmna	1.04E-92	*Cadm1*	2.20E-167	*Cd74*	5.34E-138

Figure 5 – Table Supplement 1: List of the differentially expressed genes among *Timd4*$^+$ thymic macrophages, *Cx3cr1*$^+$ thymic macrophages, and thymic monocytes. The top 100 differentially expressed genes among the three clusters are listed by their negative $\log_{10}$ transformed p-value.